

A MIXED UNCERTAINTY QUANTIFICATION APPROACH USING EVIDENCE THEORY AND STOCHASTIC EXPANSIONS

Harsheel Shah,^{1,*} Serhat Hosder,¹ & Tyler Winter²

¹*Aerospace Simulations Laboratory, Missouri University of Science & Technology, Rolla, Missouri 65409, USA*

²*M4 Engineering Inc., Long Beach, California, 90807, USA*

Original Manuscript Submitted: 02/20/2014; Final Draft Received: 10/07/2014

Uncertainty quantification (UQ) is the process of quantitative characterization and propagation of input uncertainties to the response measure of interest in experimental and computational models. The input uncertainties in computational models can be either aleatory, i.e., irreducible inherent variations, or epistemic, i.e., reducible variability which arises from lack of knowledge. Previously, it has been shown that Dempster Shafer theory of evidence (DSTE) can be applied to model epistemic uncertainty in case of uncertainty information coming from multiple sources. The objective of this paper is to model and propagate mixed uncertainty (aleatory and epistemic) using DSTE. In specific, the aleatory variables are modeled as Dempster Shafer structures by discretizing them into sets of intervals according to their respective probability distributions. In order to avoid excessive computational cost associated with large scale applications, a stochastic response surface based on point-collocation non-intrusive polynomial chaos has been implemented as the surrogate model for the response. A convergence study for accurate representation of aleatory uncertainty in terms of minimum number of subintervals required is presented. The mixed UQ approach is demonstrated on a numerical example and high fidelity computational fluid dynamics study of transonic flow over RAE 2822 airfoil.

KEY WORDS: *evidence theory, polynomial chaos, point-collocation, uncertainty quantification, computational fluid dynamics, representation of uncertainty*

1. INTRODUCTION

Uncertainty quantification (UQ) is the process of quantitative characterization and propagation of input uncertainties to the response measure of interest in experimental and computational models. Depending upon the amount of available information, researchers have been constantly trying to differentiate and characterize various forms of uncertainty. For decades, uncertainties have been segregated mainly as aleatory uncertainty (if sufficient amount of data is available such that it can be characterized with a probability distribution) and epistemic (probabilistic distributions are assumed or non-probabilistic methods are used, e.g., interval analysis). Oberkampf et al. [1] have described various methods for estimating total uncertainty by identifying all possible sources of variability, uncertainty, and error in computational simulations. As the data are sparse for an epistemic variable, there is a possibility of multiple sources of uncertainty (different information through expert opinion). This led to the formulation of mathematical structures for appropriate representation of uncertainty like the evidence theory [2], also known as the Dempster Shafer theory of evidence (DSTE). The introduction of this theory was accompanied by a discussion of merits, demerits, and different mathematical operations possible with Dempster Shafer structures [3–5].

In previous years, a number of studies have implemented and explored the concept of evidence theory. Helton et al. [6] have compared the use of several uncertainty representations like the probability theory, evidence theory,

*Correspond to Harsheel Shah, E-mail: hrsvff@mst.edu

NOMENCLATURE

n	number of random variables	\mathcal{U}	set of focal elements of \mathbb{U}
R	support region of random input variable	Bel	belief
n_p	oversampling ratio	Pl	plausibility
p	order of polynomial chaos	BPA	basic probability assignment
$\vec{\xi}$	standard input random variable vector	$m(\varepsilon)$	BPA corresponding to subset ε of \mathcal{U}
$p(\vec{\xi})$	probability density function of $\vec{\xi}$	PCE	polynomial chaos expansion
ψ	random basis function	N_t	number of terms in a total-order PCE
α	coefficient in polynomial chaos expansion	c_l	coefficient of lift
α^*	stochastic function	c_d	total coefficient of drag
μ	mean	C_p	coefficient of pressure
σ	standard deviation	M	Mach number
\mathbb{U}	universal set	$\tilde{\alpha}$	angle of attack in degrees
		Re	Reynolds number

possibility theory, and interval analysis on a range of test problems proposed as part of a workshop [7]. In the past decade, extensive research has been dedicated to improvement of the practical application of the Dempster Shafer theory due to the implicit nature of simulations and excessive computational costs. Bae et al. [8] introduced an approximation approach for uncertainty quantification using evidence theory. Their proposed algorithm includes identifying the failure region in a defined UQ space by employing an optimization routine. Specifically, the failure region in this case is considered as the region in which the limit state function for the system under consideration exceeds a particular limit state value. For example, in an analysis of a composite cantilever beam with a point load, the failure region is determined by the assessment of the likelihood that the tip displacement (limit state function) of the beam exceeds the maximum possible displacement (limit state value). Further, a surrogate model constructed using the two-point adaptive non-linear approximation (TANA2) and the multi point approximation approach (MPA) is used for repetitive simulations in UQ analysis. Later, they demonstrated the newly proposed algorithm on a large scale structure problem like the structural model of an intermediate complexity wing (ICW) [9]. Agarwal et al. [10] investigated uncertainty quantification in multidisciplinary systems analysis subject to epistemic uncertainty through the application of evidence theory. The methodology has been demonstrated using a higher-dimensional multidisciplinary aircraft concept sizing.

In view of the aforementioned developments in evidence theory for propagating epistemic uncertainty, very little attention has been given to mixed (aleatory and epistemic) uncertainty quantification using evidence theory. This is mainly due to two reasons: (1) incorporation of aleatory uncertainty in Dempster Shafer structures and (2) computational costs due to the implicit nature of simulations required for deriving evidence theory uncertainty measures. The objective of this paper is to explore the incorporation of aleatory uncertainty in Dempster Shafer structures and to implement non-intrusive polynomial chaos (NIPC), a computationally efficient stochastic response approach, for mixed uncertainty quantification using evidence theory.

Eldred and Swiler [11] have reported efficient algorithms for mixed UQ which consist of optimization based interval estimation and stochastic expansion methods. Recently, Eldred et al. [12] have demonstrated mixed UQ using DSTE by calculating evidence theory uncertainty measures for the outer loop of epistemic variables characterized by Dempster Shafer structures over the inner loop aleatory statistics. They have compared the DSTE results obtained through global optimization and sampling approach for a short column test problem. Our work focuses on representing aleatory uncertainty in terms of Dempster Shafer structures by discretizing the probability distributions into sets of intervals and treating them as epistemic variables. In order to reduce the computational costs from a simulation point of view, the NIPC [13–17] technique is employed using the Point-Collocation approach to construct a stochastic surrogate model which can replace the deterministic model in interval optimization routines for DSTE analysis.

In Section 2, we discuss different types of uncertainties that exist in a model. In Sections 3 and 4, we present the necessary mathematical framework for point-collocation NIPC and Dempster Shafer theory of evidence, respectively. Further, an approach for mixed uncertainty quantification using DSTE is presented in Section 5. A numerical analysis is performed in Section 6 in order to quantify the minimum number of subintervals required to accurately represent aleatory uncertainty within the proposed framework. The approach is demonstrated on a numerical example and a high fidelity computational fluid dynamics (CFD) study of a transonic supercritical airfoil RAE 2822 in Section 7. We conclude the paper with important interpretations of the results obtained from mixed UQ analysis using DSTE in Section 8.

2. TYPES OF UNCERTAINTY

In computational simulations, uncertainties are assigned to the specification of input physical parameters that are required for computational models. Two types of uncertainties exist in numerical modeling of physical systems: aleatory uncertainty and epistemic uncertainty.

2.1 Aleatory Uncertainty

Aleatory uncertainty, also known as probabilistic uncertainty, arises due to inherent physical variability present in the system. A specific probability distribution can be attributed to an aleatory random variable based on the data available. Aleatory uncertainty is irreducible as it is naturally present in the system under consideration. For example, the Mach number can be considered as an aleatory uncertain variable in a CFD study of airfoils or wings.

2.2 Epistemic Uncertainty

The epistemic uncertainty, also known as model-form uncertainty, arises due to lack of knowledge and is reducible by performing more experiments. The stimulant to epistemic uncertainties are the assumptions introduced in the derivation of mathematical models. This type of uncertainty cannot be defined in a probabilistic framework unless we assume a specific distribution which may lead to inaccurate results as shown by Oberkampf et al. [18]. Thus, epistemic variables are usually modeled using intervals derived from experimental data or expert judgment with the lower and the upper bound. For example, the uncertainty in the closure coefficients for a particular turbulence model used in CFD simulations can be treated as epistemic in nature.

3. POINT-COLLOCATION NON-INTRUSIVE POLYNOMIAL CHAOS

The point-collocation non-intrusive polynomial chaos is derived from the polynomial chaos theory, which is based on spectral representation of uncertainty. In previous years, many researchers have utilized polynomial chaos theory in stochastic computations. The importance of spectral representation of uncertainty lies in the fact that a stochastic response function can be decomposed into deterministic and stochastic components. Thus, for any stochastic response function α^* ,

$$\alpha^*(\vec{x}, \vec{\xi}) \approx \sum_{j=0}^P \alpha_j(\vec{x}) \psi_j(\vec{\xi}), \quad (1)$$

where $\alpha_j(\vec{x})$ is the deterministic component and ψ_j is the random basis function corresponding to the j th mode. Generally, α^* can be a function of deterministic independent variable vector \vec{x} and the n -dimensional standard random variable vector $\vec{\xi} = (\xi_1, \dots, \xi_n)$. Theoretically, Eq. (1) should include an infinite number of terms for absolute accuracy. However, for practicality purposes, a discrete sum is taken over a number of output modes. For a total order expansion, the number of output modes is given by:

$$N_t = P + 1 = \frac{(n+p)!}{n!p!}, \quad (2)$$

where p denotes the order of polynomial chaos and n is the number of random variables. The basis functions used in Eq. (1) are polynomials that are orthogonal with respect to a weight function ($p(\vec{\xi})$) over the support region (R) of the input random variable vector. In terms of convergence of statistics, the Hermite polynomial is optimal for normal distribution whereas the Laguerre and Legendre polynomials are used for exponential and uniform input uncertainty distributions, respectively. The mathematical basis for the formulation of the polynomial basis functions is well explained by Hosder et al. [14].

The main objective of the NIPC method is to obtain the polynomial coefficients without making any modification to the deterministic code, i.e., treating it as a "black box." The coefficients are solely based on deterministic code evaluations. The coefficients and orthogonality of the basis functions can be used to evaluate the statistics of the distribution for a stochastic function. For example, the zeroth mode of the expansion corresponds to the expected value of $\alpha^*(\vec{x}, \vec{\xi})$, which is given by:

$$\mu_{\alpha^*} = \bar{\alpha}(\vec{x}) = \int_R \alpha^*(\vec{x}, \vec{\xi}) p(\vec{\xi}) d\vec{\xi} = \alpha_0(\vec{x}). \quad (3)$$

Similarly, by inferring $\psi_0 = 1$ from Eq. (3), the variance of the distribution can be obtained as:

$$\sigma_{\alpha^*}^2 = \text{Var}[\alpha^*(\vec{x}, \vec{\xi})] = \int_R (\alpha^*(\vec{x}, \vec{\xi}) - \alpha_0(\vec{x}))^2 p(\vec{\xi}) d\vec{\xi} = \sum_{j=1}^P [\alpha_j^2(\vec{x}) \langle \psi_j^2(\vec{\xi}) \rangle]. \quad (4)$$

We use the fact that $\langle \psi_j(\vec{\xi}) \rangle = 0$ for $j > 0$ and $\langle \psi_i(\vec{\xi}) \psi_j(\vec{\xi}) \rangle = \langle \psi_j^2(\vec{\xi}) \rangle \delta_{ij}$. Also, the inner product of $\psi_i(\vec{\xi})$ and $\psi_j(\vec{\xi})$ in the support region R is given by:

$$\langle \psi_i(\vec{\xi}) \psi_j(\vec{\xi}) \rangle = \int_R \psi_i(\vec{\xi}) \psi_j(\vec{\xi}) p(\vec{\xi}) d\vec{\xi}. \quad (5)$$

Further, the strategy for point selection in random space for deterministic code evaluations depends upon the non-intrusive technique used. Three techniques often used are sampling based, quadrature based, and point-collocation based NIPC. In this paper, we will be focusing on using the Point-Collocation method to obtain the surrogate model.

The collocation based NIPC starts with replacing uncertain variables of interest with their polynomial expansions derived from Eq. (1). Next, $P + 1$ (N_t) vectors ($\vec{\xi}_i = \{\xi_1, \xi_2, \dots, \xi_n\}_i$, $i = 0, 1, 2, \dots, P$) are chosen in design space with a latin hypercube (LH) structure for a given polynomial chaos expansion with number of modes evaluated using Eq. (2) and the deterministic code is evaluated at these points. LH design has the advantage of improving the coverage of the design space when a small sample set is used. A linear system of equations can be obtained using the left-hand side of Eq. (1) evaluated from the solution of deterministic code at chosen random points:

$$\begin{pmatrix} \psi_0(\vec{\xi}_0) & \psi_1(\vec{\xi}_0) & \dots & \psi_P(\vec{\xi}_0) \\ \psi_0(\vec{\xi}_1) & \psi_1(\vec{\xi}_1) & \dots & \psi_P(\vec{\xi}_1) \\ \vdots & \vdots & \ddots & \vdots \\ \psi_0(\vec{\xi}_P) & \psi_1(\vec{\xi}_P) & \dots & \psi_P(\vec{\xi}_P) \end{pmatrix} \begin{pmatrix} \alpha_0 \\ \alpha_1 \\ \vdots \\ \alpha_P \end{pmatrix} = \begin{pmatrix} \alpha^*(\vec{x}, \vec{\xi}_0) \\ \alpha^*(\vec{x}, \vec{\xi}_1) \\ \vdots \\ \alpha^*(\vec{x}, \vec{\xi}_P) \end{pmatrix}. \quad (6)$$

Equation (6) represents a linear system of equations which needs to be solved in order to determine the spectral modes α_k for the stochastic function α^* . Equation (2) is considered as the minimum number of deterministic samples required to solve the linear system of equations. However, if more deterministic samples are available, the over-determined system is solved using a least squares approach. The term "over-sampling ratio" (OSR) denoted by n_p is related to Eq. (2) in the following manner:

$$N_t = n_p \times \frac{(n+p)!}{n!p!}. \quad (7)$$

Thus, an OSR of 1 corresponds to the minimum number of deterministic samples required. Hosder et al. [13] demonstrated through different stochastic model problems that an OSR of 2 is the optimum value. Once the spectral modes are evaluated, various statistics like the mean and the variance of the solution can be obtained as shown in Eqs. (3) and (4), respectively.

4. DEMPSTER SHAFER THEORY OF EVIDENCE

This section summarizes the evidence theory which is traditionally used for pure epistemic analysis. The next section will extend this idea to perform mixed UQ analysis with NIPC based stochastic expansions and convert the aleatory uncertain variables into Dempster Shafer structures.

4.1 Fundamentals of Evidence Theory

In comparison to probability theory, evidence theory introduces two new measures of uncertainty, belief (Bel), i.e., lower limit of probability, and plausibility (Pl), i.e., upper limit of probability. Evidence theory application involves the specification of $(\mathbb{U}, \mathcal{U}, m)$ where \mathbb{U} denotes the universal set, \mathcal{U} denotes the collection of subsets or set of focal elements of \mathbb{U} and m is the basic probability assignment (BPA), which can be viewed as the belief of the user of how likely it is that the uncertain input falls within the specified interval. BPA, a value between 0 and 1, can be assigned for any possible subset of the universal set based on experimentation or expert opinion. The advantage of this theory is that it does not assume any particular value within the interval nor does it assign a specific distribution to the interval.

Figure 1 illustrates that the axiom of additivity is not imposed, as the evidential measure for the occurrence and negation of an event does not have to sum to unity ($\text{Bel}(A) + \text{Bel}(\bar{A}) \leq 1$, $\text{Pl}(A) + \text{Pl}(\bar{A}) \geq 1$, $\text{Bel}(A) + \text{Pl}(\bar{A}) = 1$) where \bar{A} represents the negation of event A . According to the definition, $m(\varepsilon)$ denotes the BPA corresponding to subset ε of \mathcal{U} . Any additional evidence supporting the claim that the uncertain variable lies within a subset of ε , say $B \subset \varepsilon$, must be assigned another non-zero BPA $m(B)$. Further, $m(\varepsilon)$ should satisfy the following axioms of evidence theory:

$$\begin{aligned} m(\varepsilon) &> 0 \text{ for any } \varepsilon \in \mathcal{U}, \\ m(\varepsilon) &= 0 \text{ if } \varepsilon \subset \mathbb{U} \text{ and } \varepsilon \ni \mathcal{U}, \\ m(\emptyset) &= 0 \text{ where } \emptyset \text{ denotes an empty set,} \\ \sum m(\varepsilon) &= 1 \text{ for all } \varepsilon \in \mathcal{U}. \end{aligned}$$

Once the uncertainty associated with the domain is characterized by an evidence space in the form of BPA's, an input sample space is constructed. For example, if $y = f(\vec{x})$ where $\vec{x} = [x_1, x_2, \dots, x_n]$ with the evidence space defined as $(\mathbb{X}_i, \mathcal{X}_i, m_i)$, the input sample space is given by:

$$\mathbb{X} = \{x : x = [x_1, x_2, \dots, x_n] \in \mathbb{X}_1 \times \mathbb{X}_2 \times \dots \times \mathbb{X}_n\}. \quad (8)$$

Further for \vec{x} , the evidence space can be defined by $(\mathbb{X}, \mathcal{X}, m_X)$ where \mathcal{X} is developed from the sets contained in Eq. (9):

$$\mathcal{C} = \{\varepsilon : \varepsilon = [\varepsilon_1, \varepsilon_2, \dots, \varepsilon_n] \in \mathcal{X}_1 \times \mathcal{X}_2 \times \dots \times \mathcal{X}_n\}. \quad (9)$$

Under the assumption that the x_i are independent, m_X is defined as:

$$m_X(\varepsilon) = \begin{cases} \prod_{i=1}^n m_i(\varepsilon_i) & \text{if } \varepsilon = \varepsilon_1 \times \varepsilon_2 \times \dots \times \varepsilon_n \in \mathcal{X} \\ 0 & \text{otherwise} \end{cases}, \quad (10)$$

for subsets ε of \mathbb{X} .

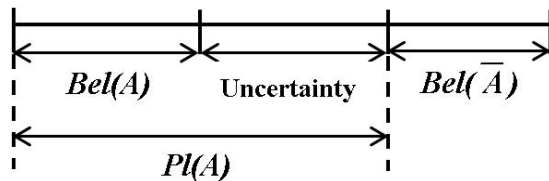


FIG. 1: Schematic of belief and plausibility.

Once the BPA's for input sample space in Eq. (8) are defined by Eq. (10), belief and plausibility for the output y with evidence space $(\mathbb{Y}, \mathcal{Y}, m_Y)$ can be evaluated as:

$$\text{Bel}_Y(\varepsilon) = \sum_{\mathcal{S} | \mathcal{S} \subseteq f^{-1}(\varepsilon)} m_X(\mathcal{S}), \quad (11)$$

$$\text{Pl}_Y(\varepsilon) = \sum_{\mathcal{S} | \mathcal{S} \cap f^{-1}(\varepsilon) \neq \emptyset} m_X(\mathcal{S}), \quad (12)$$

where $m(\mathcal{S})$ is the likelihood associated with \mathcal{S} that cannot be further assigned to specific subsets of \mathcal{S} .

As no assumptions were made to calculate these measures, Bel and Pl provide a more realistic uncertainty structure consistent with the given evidences. It is clear from Eqs. (11) and (12) that belief is the minimum likelihood associated with an event, i.e., the sum of BPA's of the propositions that totally agree with the event, and plausibility is the maximum likelihood associated with an event, i.e., the sum of BPA's of the propositions that agree partially and totally with the event. The evidence theory statistics can be summarized in terms of cumulative belief function and cumulative plausibility function (CBF and CPF) and complementary cumulative belief function and complementary cumulative plausibility function (CCBF and CCPF). Figure 2 below shows an example of these uncertainty measures obtained through the application of DSTE.

Let the uncertainty in y be characterized by the evidence space $(\mathbb{Y}, \mathcal{Y}, m_Y)$; consequently the evidence theory statistics can be defined as follows:

$$\text{CBF} = [\rho, \text{Bel}_Y(f^{-1}(\mathbb{Y}_\rho^c))], \rho \in \mathbb{Y}, \quad (13)$$

$$\text{CCBF} = [\rho, \text{Bel}_Y(f^{-1}(\mathbb{Y}_\rho))], \rho \in \mathbb{Y}, \quad (14)$$

$$\text{CPF} = [\rho, \text{Pl}_Y(f^{-1}(\mathbb{Y}_\rho^c))], \rho \in \mathbb{Y}, \quad (15)$$

$$\text{CCPF} = [\rho, \text{Pl}_Y(f^{-1}(\mathbb{Y}_\rho))], \rho \in \mathbb{Y}, \quad (16)$$

where $\mathbb{Y}_\rho = \{y : y \in \mathbb{Y} \text{ and } y > \rho\}$ and $\mathbb{Y}_\rho^c = \{y : y \in \mathbb{Y} \text{ and } y \leq \rho\}$. Detailed explanation of the evidence theory with numerical examples has been provided by Oberkampf et al. [18] and Nikolaidis et al. [19].

4.2 Rule for Combination of Evidences

Dempster Shafer theory is capable of handling data from a single source or multiple sources for an uncertain variable with the only assumption that the different sources and the random variables are independent of each other. Information from different sources is aggregated using the *rules of combination* to further evaluate the evidence theory

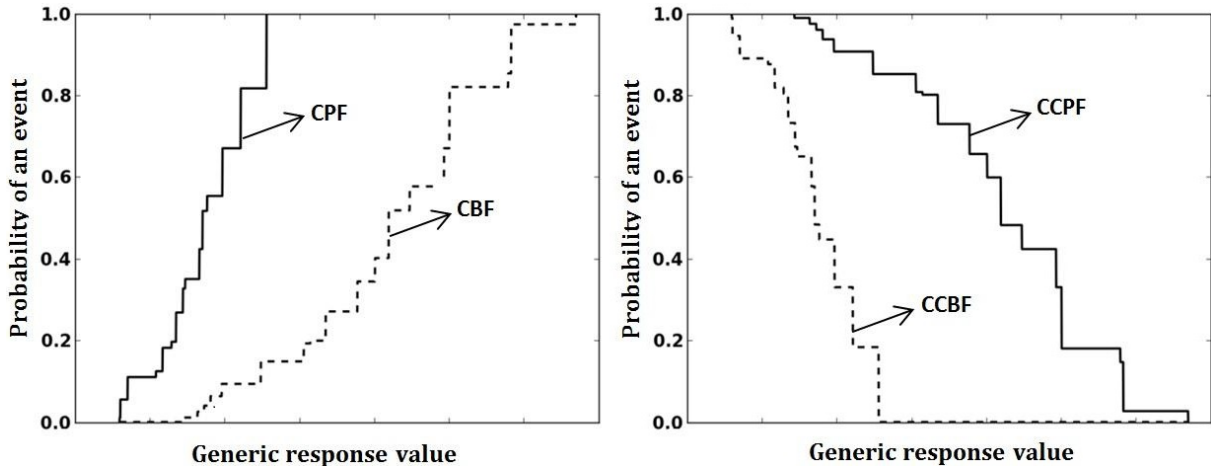


FIG. 2: Example of cumulative and complementary cumulative belief and plausibility functions.

uncertainty measures. The detailed explanation for the rules of combination is beyond the scope of this paper and can be referred from the research work of different authors [3, 5, 20]. In our study, we follow the mixing or averaging rule of combination which generalizes the averaging operation used for probability distributions. The formula for the mixing combination rule is given by:

$$m_{1\dots n}(A) = \frac{1}{n} \sum_{j=1}^n w_j m_j(A), \quad (17)$$

where m_j 's are the BPA's for belief structures being aggregated and w_j 's are the weights assigned according to the reliability of the sources. For demonstration purposes, the weights are assumed to be 1 for the examples presented in Section 6. However, Eq. (17) can be effectively used to incorporate the reliability or the confidence that can be associated with any of the sources.

5. APPROACH FOR MIXED UQ USING DSTE AND STOCHASTIC EXPANSIONS

In this section, we will describe the implementation of the stochastic response surfaces based on NIPC (Section 3) in DSTE for mixed UQ. The stochastic response surface will be used as a surrogate for the deterministic code with the overall objective of reducing original function evaluations, which can be expensive. The flow chart in Fig. 3 describes the integration procedure of NIPC into DSTE and steps to compute belief and plausibility structures.

5.1 Aleatory Uncertainty Representation in Terms of Dempster Shafer Structures

Although Dempster Shafer theory is primarily used for epistemic uncertainty quantification, there may be instances when aleatory uncertainties are present in the model along with the epistemic. One may choose to segregate the aleatory uncertainties and treat them within an inner loop in which case we may end up with multiple belief and plausibility structures as shown by Eldred et al. [12] or one may choose to discretize the aleatory variables into sets of intervals according to their respective probability distributions.

In this paper, we focus on the latter option of discretizing the aleatory variables into sets of intervals and assign BPA's to each interval based on the probability distribution. The discretization process depends upon the amount of information needed by the Dempster Shafer structure to accurately cover the uncertainty domain. For example, a random variable with uniform distribution between 0.3 and 0.7 as lower and upper bounds, respectively, can be divided into n number of intervals with an equal BPA of $1/n$ assigned to each subinterval (as shown in right plot of Fig. 4). In order to discretize a random variable with normal distribution, we need to characterize the same with a lower bound

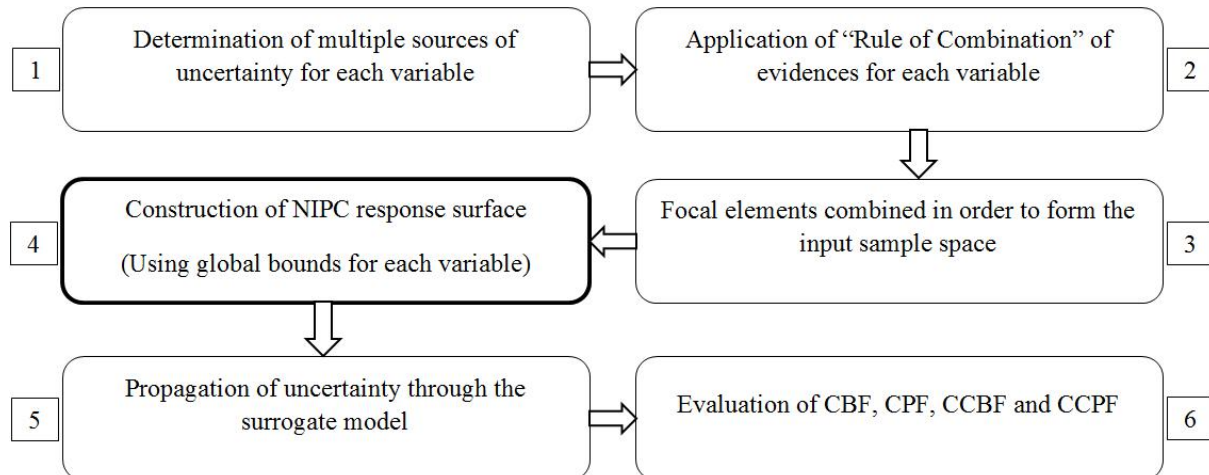


FIG. 3: Flowchart for utilization of NIPC methodology for evidence theory.

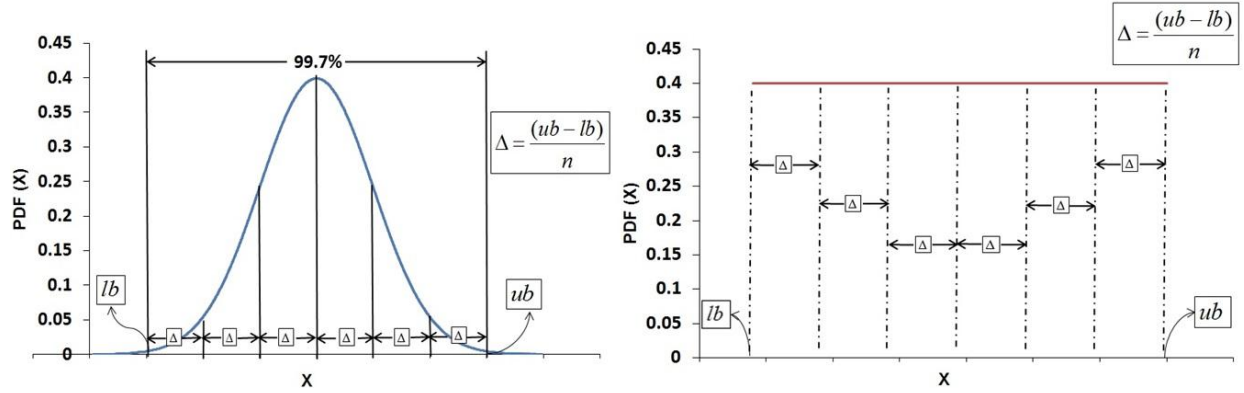


FIG. 4: Discretization of normal and uniform variable distributions; standard normal distribution with $\mu = 0$ and $\sigma = 1$ (left plot), uniformly distributed variable with lower and upper bounds [0.3, 0.7] (right plot).

and an upper bound. The left plot in Fig. 4 shows a standard normal distribution, i.e., with 0 mean ($\mu = 0$) and 1 standard deviation ($\sigma = 1$). As per the theory, for a normally distributed random variable with mean μ and σ as the standard deviation, 99.7% of the area under the curve is within $\mu \pm 3\sigma$. Hence, this can be treated as a benchmark for bounding all the normal variables in our analysis. However, the BPA should be assigned to each subinterval according to the Gaussian distribution by solving the definite integral in Eq. (18).

$$P(a < X < b) = \int_a^b f(X)dx \quad \text{where} \quad f(X) = \frac{1}{\sigma\sqrt{2\pi}} \exp \frac{-(X - \mu)^2}{2\sigma^2}, \quad (18)$$

where a and b denote the upper and lower bounds of the subinterval and $P(a < X < b)$ denotes the probability of X between a and b .

Theoretically, an infinite number of intervals for the aleatory variables with appropriate BPA's will accurately represent the uncertainty domain. However, we focus on determining the optimum number of subintervals needed to accurately represent the aleatory domain. Within a different perspective, suppose that the epistemic interval is modeled with a single interval with 100% BPA. As we increase the number of subintervals for the aleatory variable in the analysis, the results (belief and plausibility) will tend to approach the second order probability (SOP) measures (upper and lower bounds for cumulative distribution function (CDF)). The SOP [17] method uses a double loop for mixed uncertainty propagation: inner aleatory loop and outer epistemic loop. In the outer loop, a specific value for the epistemic variable is prescribed and passed on to the inner loop. Any traditional aleatory uncertainty method may then be used to perform aleatory uncertainty analysis in the inner loop. SOP provides the interval bounds for the output variable of interest at different probability levels. The SOP method is widely used for mixed uncertainty quantification with a single interval for the epistemic variable. In this paper, we utilize DSTE since it can handle multiple sources with different BPA's for the characterization of epistemic variables.

5.2 Evidence Theory Analysis

Once the aleatory variables are represented as Dempster Shafer structures, we follow the procedure described in the flow chart (Fig. 3) where the first step is to interpret data for each variable from different sources and to define a matrix for identifying intervals with non-zero evidences. These intervals are referred to as “focal elements” of each variable in DSTE terminology. The next step is to combine the evidences for each uncertain variable using Eq. (17). This will lead us to step 3 wherein we construct the input sample space in the form of different combinations of the focal elements from each uncertain variable using Eq. (8). Consequently, the composite BPA for each combination in the input sample space is evaluated using Eq. (10), which is the product of the BPA's of individual focal elements. The fourth step is to construct the stochastic surface based on point-collocation NIPC to be used as a surrogate for the

response as mentioned in Section 3. The response surface is created within the global bounds (global minimum and global maximum) for each uncertain variable. Step 5 is to propagate the uncertainty through the surrogate model which involves finding the minimum and maximum response values for each input sample space. This can be accomplished using two different approaches: sampling or optimization.

5.2.1 Sampling Approach

Akram et al. [21] compared Monte Carlo simulation and the evidence theory approach for technology portfolio planning. Their work presented the impact of sample size, uncertainty quantification method selection, and evidence combination rule selection. Helton [22] used a sampling approach for the representation of epistemic uncertainty in his work. First, hundreds of thousands of samples were chosen in the domain (e.g., for each input sample space) and the samples with minimum and maximum response values were treated as the bounds of that particular sample space. However, accuracy of the sampling approach is highly dependent on the number of samples chosen for the analysis. This method would eventually become computationally expensive with the increase in the number of variables and the uncertainty information per variable. To overcome the computational costs, we implement the optimization procedure to find the minimum and maximum response.

5.2.2 Interval Optimization Approach (Implemented in the Proposed Methodology)

As the epistemic uncertainties are characterized by lower and upper bounds, we perform bound-constrained optimization within each input sample space. Limited memory Broyden-Fletcher-Goldfarb-Shanno bound constrained optimization (L-BFGS-B [23]); a local gradient-based solver is used for interval minimization and maximization which uses the BFGS update to approximate the inverse Hessian matrix. Thus, we perform two different optimizations: one for the minimum response and the other for the maximum response. This procedure is computationally efficient as compared to the sampling approach and also the accuracy is improved. An important point to note is that we perform the optimization using the surrogate model which further reduces the computational cost. The uncertain variables are transformed into their respective standard random variable bounds within each input sample space before the optimization procedure. Mathematically, the bound constrained problem can be expressed as follows:

$$\begin{aligned} & \text{minimize/maximize} && f(\vec{\xi}), \\ & \text{subject to} && \vec{\xi}_L \leq \vec{\xi} \leq \vec{\xi}_U, \end{aligned}$$

where $f(\vec{\xi})$ is the required response value, $\vec{\xi}_L$ and $\vec{\xi}_U$ correspond to lower and upper bounds of the standard random variable. The final step is to calculate the belief and plausibility structures using the minimum and maximum response values according to Eqs. (11) and (12).

The advantage of using NIPC as the surrogate of the response can be understood especially for high fidelity simulations if the output statistics are approximated accurately with a second degree polynomial. In such cases, we can directly use Newton's optimization method which would require one iteration to optimize the NIPC response surface due to its Taylor series approximation. In this manner, we can even reduce the NIPC function evaluations along with the original function evaluations.

6. ANALYSIS FOR OPTIMUM DISCRETIZATION OF ALEATORY VARIABLES

In order to provide a baseline for discretization of an aleatory uncertain variable and quantify the number of subintervals required to accurately represent the aleatory uncertainty, a numerical analysis based on mixed UQ using evidence theory is presented. Numerous combinations of uncertain variables (normal or uniform) have been adopted for the analysis in two multidimensional test functions; (1) exponential function and (2) Runge function. These problems have been widely used as challenge problems due to the inherent nature of variation which is feasible for any optimization algorithm testing. A stochastic response surface based on point-collocation NIPC as explained in Section 3

is implemented as the surrogate model for each of the test functions. At first, NIPC order convergence is achieved in order to demonstrate the efficiency of DSTE with NIPC.

Mathematically, the two test functions are given by:

Exponential function

$$Y1 = f1(\vec{x}) = \exp \left\{ - \sum_{i=0}^{n-1} \frac{1}{i+1} x_i \right\}, \quad (19)$$

Runge function

$$Y2 = f2(\vec{x}) = \frac{1}{1 + \sum_{i=1}^n x_i^2}, \quad (20)$$

where n represents the number of random variables.

6.1 NIPC Order Convergence

We study the NIPC order convergence with the exponential function in Eq. (19) including 8 input variables (x_i with $i = 0, 1, \dots, 7$) and the Runge function in Eq. (20) consisting of input variables (x_i with $i = 1, 2, \dots, 4$), characterized by purely epistemic multiple source uncertainty. $Y1$ and $Y2$ denote the system responses, respectively. The input uncertainty information for both test functions is given in Tables 1 and 2.

The evidence theory analysis is carried out for both test functions as explained in Section 5–5.2. There are 7680 and 96 combinations in the input sample space structure for the exponential and the Runge function, respectively. The NIPC response surface was constructed based on the global bounds for each uncertain variable. For example, x_0 in Table 1 has 2 sources of uncertainty with 1 interval from the first source and 3 intervals from the second. Using these intervals, we choose the global minimum, i.e., 0.1 as the lower bound and the global maximum, i.e., 0.9 as the upper bound for x_0 . Similarly, choosing the global bounds for the other variables, NIPC order convergence analysis is conducted. An over-sampling ratio of 2 is utilized and the linear system of equations in Eq. (6) is solved using the least squares approach. The DSTE analysis results for both test problems are presented in Fig. 5.

TABLE 1: Input uncertainty information for the exponential function. The format for uncertainty information is: [lower bound, upper bound] BPA (%)

Variable	Source 1	Source 2	Source 3
x_0	[0.6, 0.9] 100%	[0.1, 0.3] 33%, [0.4, 0.6] 34%, [0.5, 0.9] 33%	—
x_1	[0.2, 0.3] 50%, [0.4, 0.5] 50%	[0.0, 0.6] 70%, [0.5, 0.9] 30%	[0.1, 0.4] 100%
x_2	[0.1, 0.5] 40%, [0.6, 0.9] 60%	[0.3, 0.8] 100%	[0.4, 0.5] 100%
x_3	[0.1, 0.4] 100%	[0.3, 0.7] 100%	—
x_4	[0.2, 0.4] 100%	[0.5, 0.8] 20%, [0.7, 0.9] 80%	—
x_5	[0.1, 0.3] 100%	[0.2, 0.5] 100%	[0.3, 0.6] 30%, [0.7, 1.0] 70%
x_6	—	[0.1, 0.5] 100%	[0.3, 0.6] 100%
x_7	[0.2, 0.8] 100%	—	[0.7, 0.9] 100%

TABLE 2: Input uncertainty information for the Runge function

Variable	Source 1
x_1	[0.6, 0.9] 30%, [0.2, 0.4] 20%, [0.1, 0.5] 40%, [0.9, 1.0] 10%
x_2	[2.1, 3.5] 30%, [1.5, 3.0] 40%, [1.0, 2.0] 30%
x_3	[0.12, 0.25] 20%, [0.3, 0.6] 25%, [0.1, 0.4] 15%, [0.5, 0.9] 40%
x_4	[0.4, 0.6] 40%, [0.3, 0.8] 60%

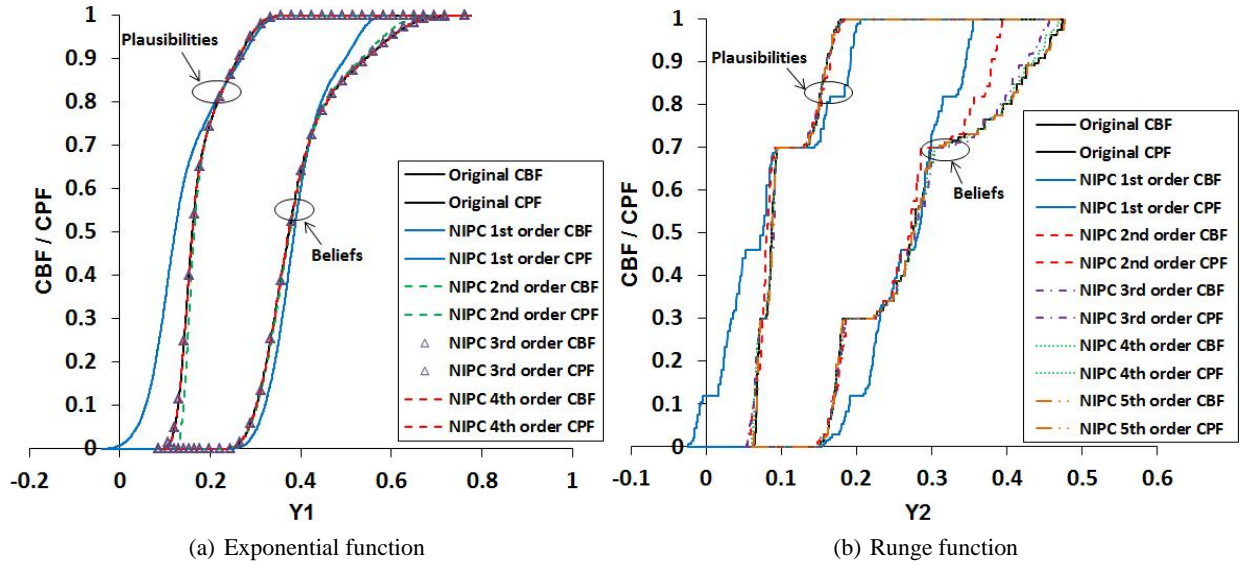


FIG. 5: Results for DSTE with NIPC.

It is evident that as the polynomial degree increases, the accuracy of the approximation increases. In order to quantify accuracy, we define error in area as the integral of absolute difference between the original function value $Y_{org}(z)$ and NIPC response value $Y_{nipc}(z)$ at the z th belief/plausibility level. Mathematically it can be represented as given in Eq. (21) and the integral is evaluated numerically. Further, the error is scaled with respect to the error in first order NIPC approximation.

$$\text{Error} = \int_0^1 |Y_{org}(z) - Y_{nipc}(z)| dz. \quad (21)$$

Error convergence plots are shown in Fig. 6. The 95% confidence interval (CI) is evaluated in terms of belief and plausibility measures. The lower bound of CI is represented by the response value at 2.5% plausibility level and the

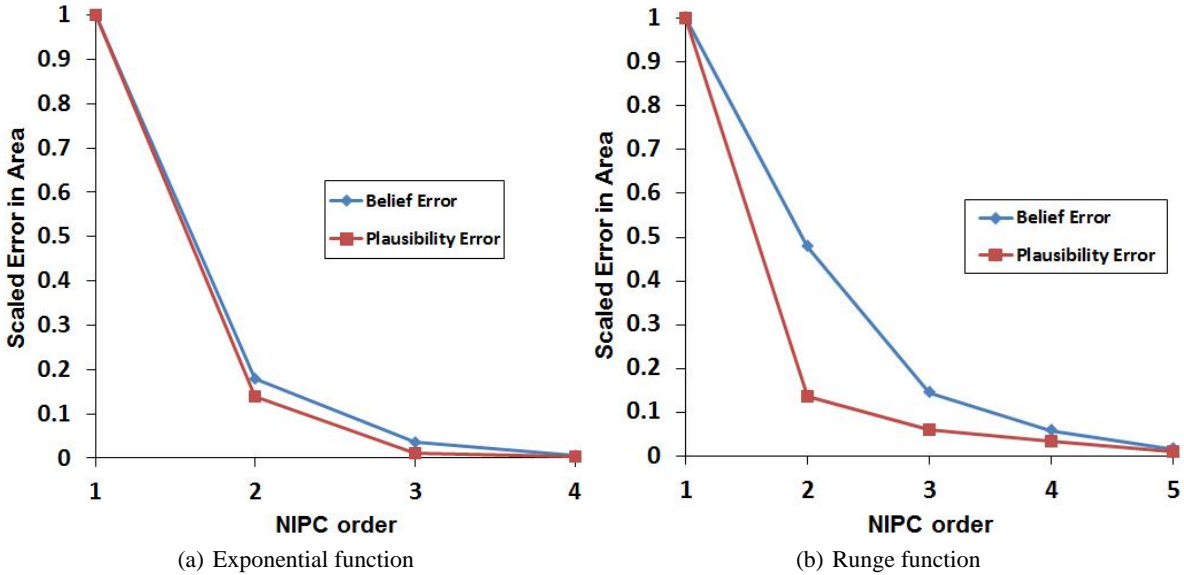


FIG. 6: Error convergence results using Eq. (21).

upper bound is indicated by 97.5% belief level. Table 3 gives the convergence summary for different NIPC orders as compared to the original function statistics.

Based on the results of the polynomial order convergence study, we shall use a third-order expansion for the exponential function and a fourth-order expansion for the Runge function in further analysis for computational efficiency as the results are within acceptable limits of accuracy for demonstration purposes (<4% difference). It is certain that the final results for the minimum number of discretized intervals required for an aleatory variable will not be affected. 330 original function evaluations are needed to construct an inexpensive third-order NIPC response surface for the exponential function over the uncertainty domain as opposed to 82,496 crude deterministic evaluations. Similarly, 140 original function evaluations will be needed in order to represent the Runge function accurately. Thus, point-collocation NIPC is an effective and computationally efficient uncertainty propagation tool even in case of multiple sources of uncertainties.

6.2 Optimum Number of Intervals for Representing Aleatory Domain

This study will provide an overview of different parameters affecting the number of subintervals needed to accurately represent aleatory variables in terms of Dempster Shafer structures. These parameters are as listed below:

1. Number of aleatory variables
2. Number of epistemic variables
3. Number of sources for epistemic variables
4. Distribution of the aleatory variables (normal and uniform distributions studied in this paper)

Different cases considered for the numerical analysis are summarized in Table 4. Note that cases 1, 2, 4, and 5 are with single source epistemic uncertainty with 100% BPA. These cases are specifically chosen so as to be compared

TABLE 3: Convergence of 95% CI with NIPC order

Case (Response used in optimiza- tion)	Exponential function			Runge function		
	# of original function evalua- tions	95% CI results	% Difference	# of original function evalua- tions	95% CI results	% Difference
Original function	82496	[0.1151, 0.6348]	—	1046	[0.0645, 0.4729]	—
order 1	18	[0.0209, 0.5421]	[138.53, 15.75]	10	[-0.0160, 0.3548]	[162.46, 28.54]
order 2	90	[0.1325, 0.6170]	[14.05, 2.84]	30	[0.0548, 0.3927]	[11.42, 18.53]
order 3	330	[0.1125, 0.6310]	[2.28, 0.60]	70	[0.0558, 0.4541]	[10.18, 4.06]
order 4	990	[0.1154, 0.6344]	[0.26, 0.06]	140	[0.0613, 0.4669]	[3.63, 1.28]
order 5	—	—	—	252	[0.0632, 0.4754]	[1.46, 0.53]

TABLE 4: Combination of uncertain variables studied for optimum interval discretization

Case	Description
1	1 Epistemic (single source with 100% BPA) and 1 aleatory variable
2	1 Epistemic (single source with 100% BPA) and multiple aleatory variables (2, 4, 6, and 8)
3	1 Epistemic (multiple sources) and 1 aleatory variable
4	2 Epistemic (single source with 100% BPA each) and 1 aleatory variable
5	2 Epistemic (single source with 100% BPA each) and 2 aleatory variables
6	2 Epistemic (multiple sources) and 2 aleatory variables

with the SOP results and present the error convergence based on Eq. (21). For cases 3 and 6, which exhibit multiple source epistemic uncertainty, the analysis is based on the asymptotic convergence of relative error between successive iterations as we increase the number of subintervals for the aleatory variable. Table 5 provides the uncertainty information for both test problems.

Evidence theory analysis using NIPC response surface is carried out for each case, starting with the particular number of subintervals for aleatory variables. For iterative convergence, we start with 5 subintervals for each aleatory variable in the case of 1, 2, and 4 aleatory variables per analysis and increase it by 5 at every iteration. Similarly, in the case of 6 and 8 aleatory variables, we start with 2 subintervals. The difference in choosing the initial number of subintervals is due to the fact that the combined BPA of more number of variables is expected to be smaller due to the multiplicative effect for the product space expressed in Eq. (10). As two aleatory distributions are studied in this paper, the mathematical functions are tested for each case with 1 aleatory distribution at a time which will enable us to compare the interval discretization for both distributions.

6.2.1 An Exponential Decay Model for Predicting Error Convergence

As the number of aleatory variables increases, the analysis for error convergence becomes more and more expensive in terms of number of combinations in the input sample space. This subsection will describe an exponential decay model which can predict the convergence based on the initial 3 to 4 error evaluations. This is especially useful in problems with higher dimensions which are computationally expensive otherwise. For example, in the present analysis, the decay model is used to predict the error convergence for the cases with 4, 6, and 8 aleatory variables. The decay model is given by:

$$Err_p = E_0 \times \frac{1}{1 - \exp(-N/k)}, \quad (22)$$

where Err_p is the predicted error, E_0 and k are constants based on initial error evaluations, and N is the number of subintervals.

The constants are evaluated by minimizing the sum of squares of differences between the initial error evaluations and predicted error values for the same number of subintervals. A generalized reduced gradient (GRG) solver was used to minimize the sum of squares in this analysis. Once they are evaluated, the error prediction model can be used for different number of intervals N , being the only variable in Eq. (22).

TABLE 5: Uncertainty information for the cases described in Table 4 ($k = 0$ for exponential function and $k = 1$ for Runge function)

Case	Aleatory uncertainty [Number of subintervals per variable per iteration]	Epistemic uncertainty
1	$x_k: N(2.5, 0.15)$ or $U(3.5, 5.5)$ [5, 15, 50, 75, 100, 125]	$x_{k+1} : [0.1, 1.0] 100\%$
2	x_k to $x_i (i = 2, 4, 6, 8)$ $N(2.5, 0.15)$ or $U(0.5, 1.5)$ For $i = 2 : [5, 15, 50, 75, 100, 125]$ For $i = 4 : [5, 10, 15, 25, 30, 35]$ For $i = 6 : [2, 4, 6, 8, 10]$ For $i = 8 : [2, 3, 4, 5]$	$x_p : [0.1, 1.0] 100\%$ p : total number of variables
3	$x_k: N(2.5, 0.15)$ or $U(3.5, 5.5)$ [5, 15, 50, 75, 100, 125]	$x_{k+1} : [0.1, 0.4] 30\%, [0.3, 0.7] 40\%, [0.8, 0.9] 30\%$
4	$x_k: N(2.5, 0.15)$ or $U(3.5, 5.5)$ [5, 15, 50, 75, 100, 125]	$x_{k+1} : [0.1, 1.0] 100\%$ $x_{k+2} : [2.0, 3.5] 100\%$
5	x_k and $x_{k+2} N(2.5, 0.15)$ or $U(3.5, 5.5)$ [5, 15, 50, 75, 100, 125]	$x_{k+1} : [0.1, 1.0] 100\%$ $x_{k+3} : [2.0, 3.5] 100\%$
6	x_k and $x_{k+2} N(2.5, 0.15)$ or $U(0.5, 1.5)$ [5, 15, 50, 75, 100, 125]	$x_{k+1} : [0.1, 0.4] 20\%, [0.35, 0.6] 40\%, [0.7, 1.2] 40\%$ $x_{k+3} : [0.2, 0.5] 30\%, [0.9, 1.5] 40\%, [0.6, 1.0] 30\%$

Figures 7 and 8 show the error convergence for both test functions in terms of increasing subintervals. The most important parameter affecting the choice of number of subintervals is the number of aleatory variables in the design problem. The other three parameters, i.e., distribution of aleatory variables, number of sources for the epistemic variables, and number of epistemic variables seemed to have minimal effect with decreasing order of sensitivity. It can also be inferred that the increase in number of subintervals, and thereby the accuracy of the approximation, will be accompanied with increased computational time and effort. Thus, a trade-off needs to be made between the required accuracy and the computational efficiency.

In the case of 1 and 2 aleatory variables, deciding the number of subintervals required is straightforward as the number of intervals at which the convergence achieved is evident. For higher dimensions, i.e., 4, 6, and 8 variable cases, we choose the minimum number of subintervals at a point where there is approximately 90% reduction in error as compared to the first iteration. Increasing the number of intervals beyond this point will be considered infeasible in terms of reduction in error with significant increase in number of combinations for DSTE analysis.

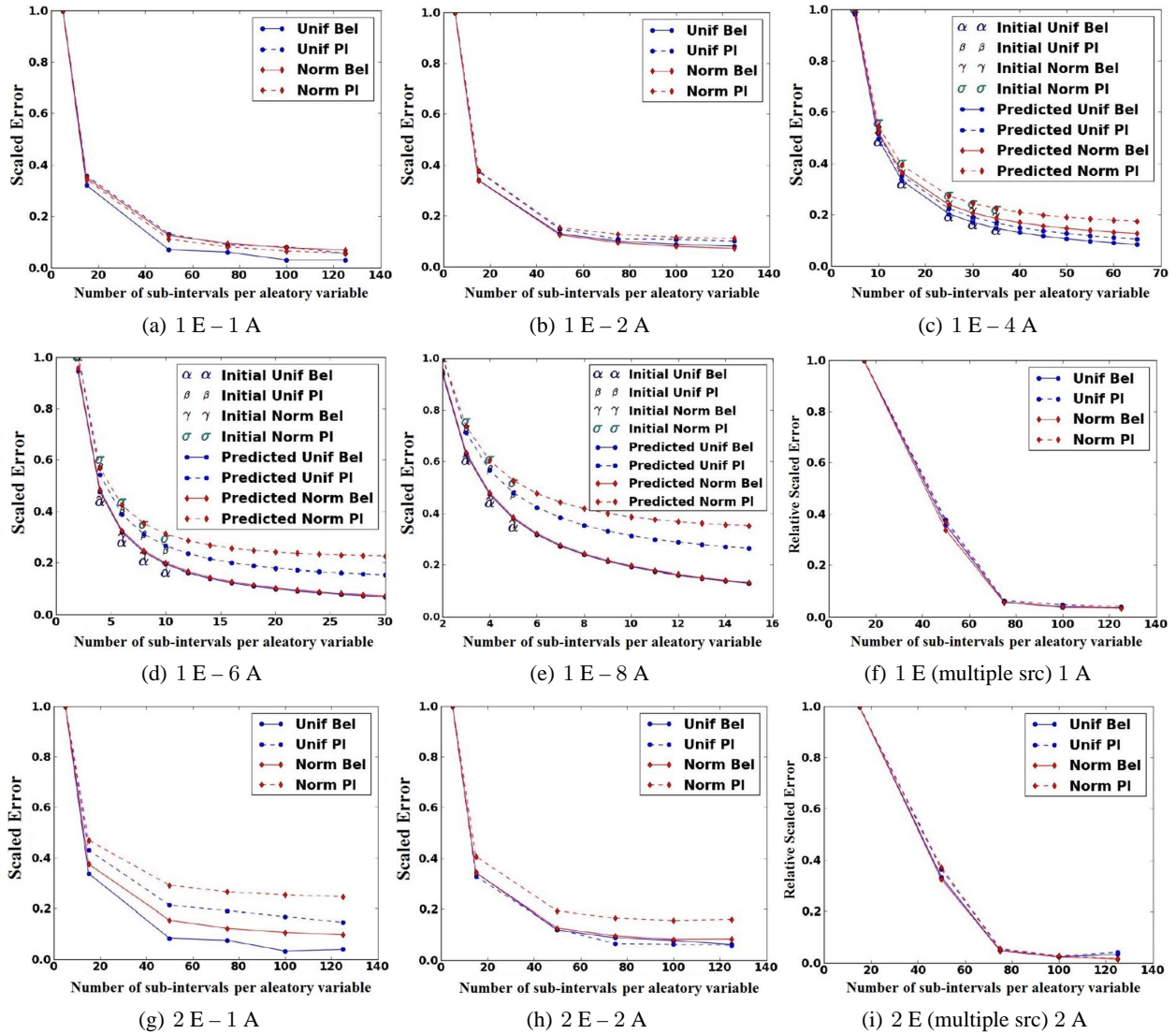


FIG. 7: Exponential function error convergence (1)–(9) with normal and uniform distributions for aleatory variables (E: epistemic variable, A: aleatory variable).

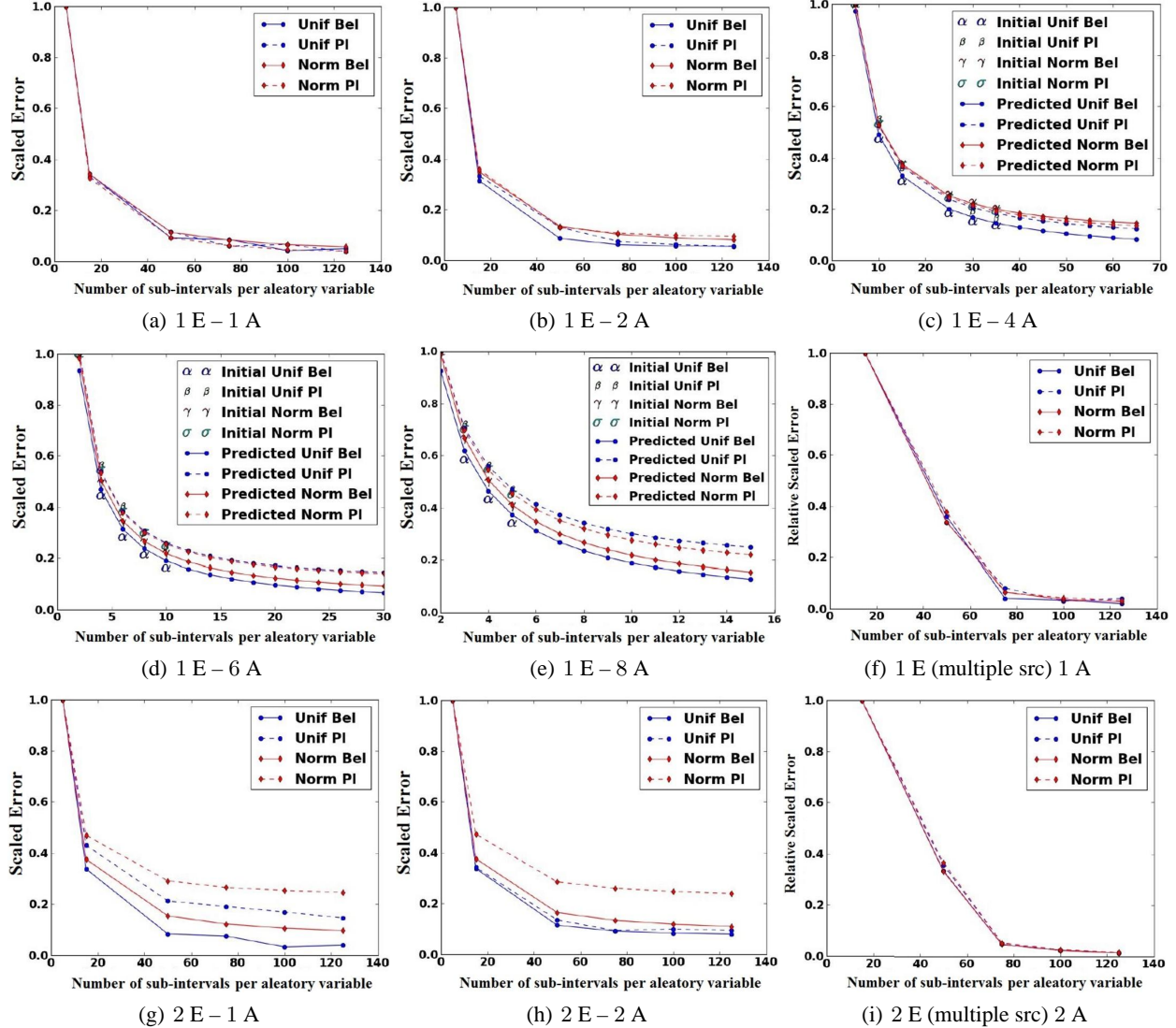


FIG. 8: Runge function error convergence (1)–(9) with normal and uniform distributions for aleatory variables (E: epistemic variable, A: aleatory variable).

Table 6 lists the optimum number of subintervals for each case which is the minimum recommended to cover the aleatory uncertainty domain. In the case of an odd number of uncertain aleatory variables, the optimum number of subintervals can be evaluated using interpolation. The optimum number of subintervals should be interpreted as a good enough approximation to accurately represent an uncertain aleatory variable. The accuracy can always be improved by taking more number of subintervals per variable and/or by increasing the ± 3 standard deviation limit to ± 6 for a normal random variable if the computational architecture permits. In case of a huge number of uncertain variables, advanced dimension reduction techniques based on sensitivity analysis may be adopted.

6.3 The Effect of the Distribution Type on Aleatory Interval Discretization

As the distributions of aleatory variables vary, the contribution of each discretized interval also varies. Error convergence plots in Figs. 7 and 8 imply two mathematical conclusions: (1) the error while discretizing the uniform variable

TABLE 6: Optimum number of intervals for each case

Description	N_{opt}
1 Epistemic (single source with 100% BPA) and 1 aleatory variable	75
1 Epistemic (single source with 100% BPA) and multiple aleatory variables (2, 4, 6, and 8)	(50, 40, 20, and 12, respectively)
1 Epistemic (multiple sources) and 1 aleatory variable	75
2 Epistemic (single source with 100% BPA each) and 1 aleatory variable	75
2 Epistemic (single source with 100% BPA each) and 2 aleatory variables	50
2 Epistemic (multiple sources) and 2 aleatory variables	50

is less as compared to that of the normal variable due to the truncation effect at the tail region, and (2) after a certain number of subintervals, the rate of decrease in error is not as prominent for a normal variable as compared to a uniform variable. This is mainly due to the fact that as the number of subintervals increases, the resulting BPA's for most of the intervals are derived from the tail regions which have a minimal probability value.

In case there are random variables with different distributions in the design problem, which is the most practical case, a relation can be proposed to identify the number of subintervals for each distribution:

$$\tilde{N}_{opt} = \frac{N_{opt}}{\text{number of distributions}}, \quad (23)$$

where \tilde{N}_{opt} represents the number of subintervals for each distribution, N_{opt} corresponds to the case of total number of aleatory variables in the problem under consideration, and “number of distributions” in this paper is adopted as 2. This proposition is based on the numerical experiments performed in the previous section where two types of distributions were studied (normal and uniform). Each of these distributions represented the complete aleatory domain in the problem. In case of multiple distributions in a specific problem, the aleatory domain is shared by those distributions and hence the optimum number of intervals required to represent the domain can be divided between the participating distributions.

Now the question is which distribution should be given more preference in terms of number of intervals in case of multiple distributions? Using the fact that the normal variable contributes less as compared to a uniform variable with the same number of subintervals and based on the numerical analysis performed, the required number of subintervals can be reduced for the normal variable by approximately 20% of N_{opt} . For example, evaluating Eq. (23) for a specific problem yields an \tilde{N}_{opt} of say 25, the required number of subintervals for the normal variable can be reduced by $25 \times 0.2 = 5$ intervals, i.e., the variable divided into 20 subintervals. However, in order to cover the aleatory domain after the correction for the normal variable, we increase the number of subintervals for the uniform by the same amount (i.e., \tilde{N}_{opt} for uniform variable will be 30). This point will be clear in the next subsection and Section 7 where the implementation of Eq. (23) is demonstrated and verified.

6.4 Demonstration of Difference Between DSTE and Pure Interval Analysis

One approach in epistemic uncertainty quantification is to approximate the range of output uncertainty by adopting the interval defined by the global minimum and maximum of the input uncertainty. Ignoring the multiple sources of information for the input uncertainty may provide a conservative estimation of the output uncertainty. This subsection provides a comparison between pure interval analysis and the evidence theory with the proposed methodology. The Runge test function is reconsidered with the uncertainty information as presented in Table 7.

Two different analyses are carried out for the above problem: (1) SOP analysis by choosing global bounds for both the epistemic variables (i.e., [1.5, 3.0] for x_2 and [0.2, 0.85] for x_3), and (2) evidence theory analysis for mixed uncertainty incorporating the information from the sources. Note that for both methods; SOP and DSTE, a fourth-order chaos expansion was chosen in order to propagate the uncertainty. The number of original function evaluations required were 140, evaluated using Eq. (7) with an OSR of 2. Ideally, using Eq. (23), we calculate \tilde{N}_{opt} as 25 which corresponds to the number of subintervals needed for each distribution. After the correction is implemented

TABLE 7: Input uncertainty information for the Runge function for comparison with pure interval approximation

Variable	Distribution	Uncertainty information
x_1	Uniform	(0.5, 1.5)
x_2	Epistemic	Source 1: [1.5, 2.0] 30%, [1.7, 2.5] 40%, [2.1, 3.0] 30%
x_3	Epistemic	Source 1: [0.2, 0.6] 70%, [0.55, 0.85] 30%
x_4	Normal	(2.5, 0.15)

for the normal variable, the numbers of subintervals are obtained as 20 and 30 for normal and uniform, respectively.

For the purpose of convergence demonstration, five different cases for number of subintervals summarized in Table 8 with results plotted in Fig. 9. It shows that the interval analysis provides us with a conservative or over-prediction of the uncertainty range. However, an important point to note is that the global bounds of the uncertainty range do match with the pure interval analysis results, which is due to the fact that the uncertainty domain (i.e., the minimum and maximum bound) is unchanged. The response values using DSTE analysis and pure interval analysis are compared at different levels in Table 9.

TABLE 8: Number of intervals for aleatory variables

Case	Normal	Uniform
1	2	5
2	5	10
3	10	15
4	20	30
5	25	40

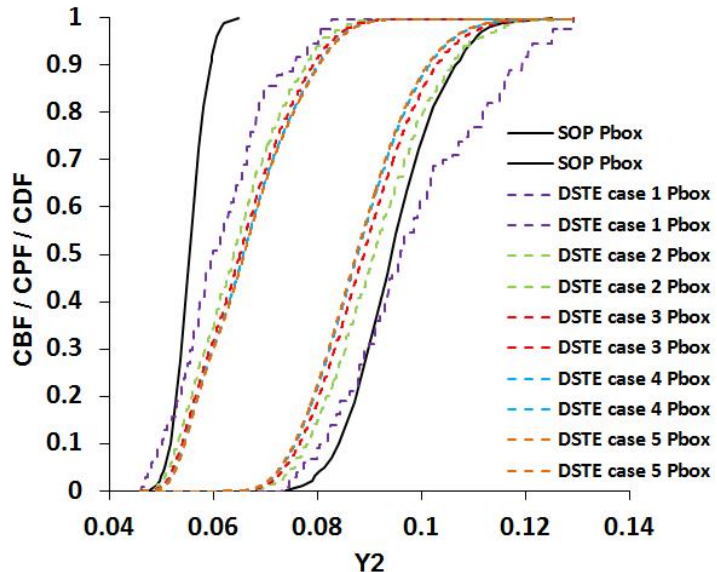


FIG. 9: SOP and DSTE results for Runge function.

TABLE 9: UQ results for the Runge function

Probability/belief/ plausibility level	Pure interval analysis [lower bound, upper bound]	DSTE analysis [plausibility, belief]
0	[0.04765, 0.07377]	[0.04611, 0.06754]
2.5%	[0.04987, 0.07926]	[0.05167, 0.07101]
25%	[0.05337, 0.08847]	[0.05835, 0.08092]
50%	[0.05543, 0.09429]	[0.06577, 0.08768]
75%	[0.05746, 0.10031]	[0.07316, 0.09489]
97.5%	[0.06108, 0.11235]	[0.08624, 0.10911]
100%	[0.06477, 0.12489]	[0.09241, 0.12915]

7. DEMONSTRATION OF MIXED UQ USING EVIDENCE THEORY

7.1 Rosenbrock Function

Before we demonstrate the mixed UQ approach on a CFD problem, we test the conclusions for the selection of the optimum number of subintervals on a numerical problem, which includes the Rosenbrock function as the response. It is a smooth nonlinear function for which the generalized formulation is given as:

$$f(\vec{x}) = \sum_{i=1}^{n-1} [(1 - x_i)^2 + 100(x_{i+1} - x_i^2)^2], \quad (24)$$

where n represents the number of uncertain variables. For this problem, we choose $n = 3$. The uncertainty information is as given below in Table 10:

A fourth-order chaos expansion was chosen to model the uncertainty propagation with the NIPC response surface. The number of original function evaluations required was 70, evaluated using Eq. (7) with an OSR of 2. The DSTE analysis results obtained with the mixed UQ approach for the Rosenbrock function are given in Fig. 10. With the objective to demonstrate the convergence, Table 11 lists the different cases considered in terms of number of subintervals and compares the response intervals at two different levels: 2.5% and 97.5%. The percent differences between successive iterations give an overview of the convergence as we move towards the optimum number of intervals for the case of 2 aleatory variables ($N_{opt} = 50$). Case (3) seems to provide comparable results with case (4) and the number of combinations is also decreased from 6125 to 4200. Thus, choosing the optimum number of intervals as explained in Section 6–6.2 and 6–6.3 does provide the uncertainty results with desired accuracy and efficiency.

7.2 Transonic Flow Over RAE 2822 Airfoil

To demonstrate the mixed UQ approach based on DSTE and stochastic expansions on a high fidelity CFD problem, we study steady, two-dimensional, viscous, turbulent flow over RAE 2822 airfoil subject to mixed (aleatory and epistemic) input uncertainties. Witteveen et al. [24] have previously compared the stochastic collocation (SC) method based on Gauss quadrature to the simplex elements stochastic collocation (SESC) method for transonic flow UQ analysis over RAE 2822. This paper will focus on using the mixed UQ with DSTE approach through interval discretization for the

TABLE 10: Input uncertainty information for the Rosenbrock function

Variable	Distribution	Uncertainty information
x_1	Uniform	[-2.048, 2.048]
x_2	Normal	($N[0.215, 0.04]$)
x_3	Epistemic	Source 1: [-3.7, 2.0] 50%, [1.5, 4.5] 50% Source 2: [0.0, 2.5] 33.34%, [-5.0, -1.7] 33.33%, [3.7, 5.0] 33.33% Source 3: [1.25, 4.15] 35%, [-2.9, 1.4] 65%

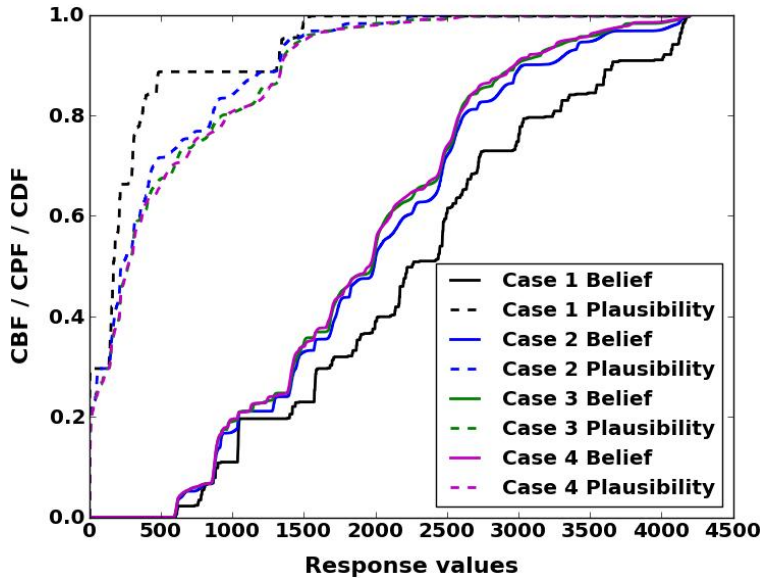


FIG. 10: Mixed UQ results for Rosenbrock function.

TABLE 11: Mixed UQ convergence results for Rosenbrock function analysis

Discretization				Response intervals at different levels			
Case	Normal	Uniform	# of Combinations	2.5%	% Difference	97.5%	% Difference
1	5	5	175	[0.816, 759.42]	—	[1489.86, 4149.45]	—
2	15	15	1575	[1.181, 613.60]	[36.55, 21.24]	[1748.01, 4050.18]	[15.94, 2.42]
3	20	30	4200	[1.376, 611.43]	[15.25, 0.35]	[1808.07, 3720.43]	[3.38, 8.49]
4	25	35	6125	[1.456, 611.25]	[5.65, 0.029]	[1852.79, 3696.77]	[2.44, 0.64]

aleatory variables with NIPC as the surrogate model for the response variables of interest. The CFD code used in this study for numerical solution of steady Reynolds-averaged-Navier-Stokes (RANS) equations is ANSYS FLUENT 13.0 [25]. The Mach number and the angle of attack have been treated as aleatory uncertainties. One of the closure coefficients used in the Spalart-Allmaras [26] turbulence model is treated as an epistemic uncertainty with multiple sources of information.

7.2.1 CFD Model and Grid Convergence

The geometry of RAE 2822 airfoil is defined by the design airfoil coordinates tabulated in Cook et al. [27]. A suitable computational mesh size for stochastic simulations is selected by performing a grid convergence study. The grid convergence analysis is performed for the flow conditions corresponding to Case 6 in Cook et al [27] with $M_\infty = 0.725$, $\tilde{\alpha} = 2.92^\circ$, and $Re = 6.5$ million (wind tunnel corrected values are $M_\infty = 0.729$ and $\tilde{\alpha} = 2.31^\circ$). A second-order spatial discretization is used along with the Roe flux difference splitting scheme. The iterative convergence is achieved through the reduction of the residuals of the governing equations by six orders of magnitude.

Four grid levels are generated for the grid convergence. The finest grid (level 4) consists of 86,400 quadrilateral cells with a mesh size of 721×121 . The chord length for the airfoil is 1.0 ft with 589 points on the airfoil surface and 66 in the wake region. The far-field is 27 ft away from the trailing edge and the ratio of outer boundary distance to the wake distance is 0.75. The coarser grids (levels 3, 2, and 1) are obtained by halving the number of points in the streamwise and normal direction. Thus, grid levels 3, 2, and 1 are represented by 361×61 , 181×31 , and 91×16

mesh sizes, respectively. Figure 11 shows the third grid level selected after the convergence study, which is used for further analysis. The pressure distribution of the deterministic simulations for all the grid levels is compared with the experimental results of Case 6 in Fig. 12 along with the estimation of the discretization error for the drag coefficient calculated by the Richardson extrapolation technique explained by Hosder et al. [28].

7.2.2 Stochastic Problem Description

For this study, the Mach number (M) and the angle of attack (α) have been treated as aleatory variables with uncertainty in the form of normal distributions with the mean values corresponding to the experimental conditions for Case

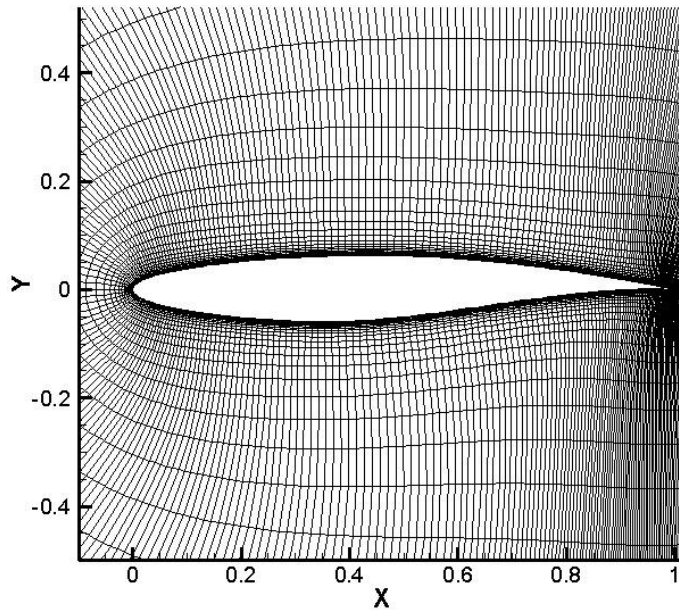


FIG. 11: Grid around the airfoil (grid level 3).

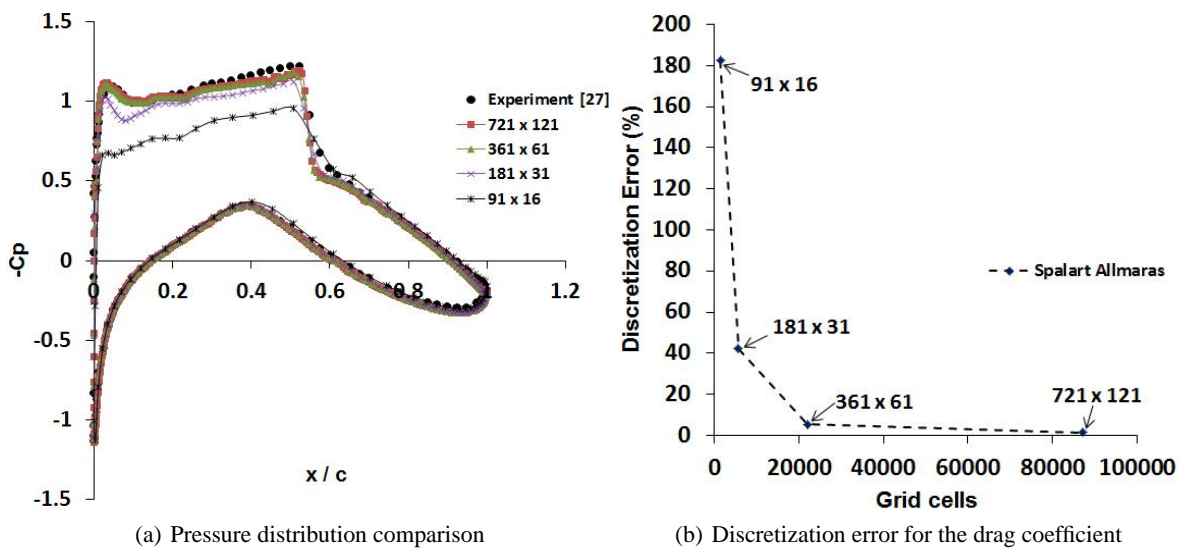


FIG. 12: Grid convergence results.

6 in Cook et al. [27] whereas the standard deviations are $\sigma_M = 0.005$ and $\sigma_\alpha = 0.1$, respectively. One of the closure coefficients used in the Spalart-Allmaras turbulence model is treated as an epistemic uncertainty.

The standard form of the Spalart-Allmaras model consists of various closure coefficients such as C_{b1} , C_{b2} , C_{v1} , σ_{SA} , C_{w2} , and C_{w3} , a detailed description of which can be found in Spalart and Allmaras [26]. The variation in these parameters has been studied in detail by many researchers. Recently, Kato and Obayashi [29] proposed an approach for uncertainty in turbulence modeling based on assimilation technique. They claim that the original values proposed by the model proposer were statistically accurate for the closure coefficients. Godfrey and Cliff [30] derived the sensitivity equations for turbulent flow simulations for different turbulence models. In their study, the Spalart-Allamaras model analysis showed that the most influential coefficients in order of decreasing sensitivity magnitude are C_{v1} , C_{b1} , σ_{SA} , and C_{w2} . The other coefficients C_{b2} and C_{w3} had minimal effect on the output quantity studied.

In this work, the top three sensitive parameters were tested using the wind tunnel corrected conditions within the bounds obtained with a coefficient of variance (CoV) of approximately 9% from their baseline values (i.e., $C_{v1} = 7.1$, $C_{b1} = 0.1355$, and $\sigma_{SA} = 2/3$). The variation in closure coefficients was mainly based on the ranges adopted in previous research work by Rhee [31] and Cheung et al. [32]. The pressure coefficient on the airfoil surface was monitored for all the simulations and the results showed that the shock region on the upper surface was the most critical region being affected by the variation in closure coefficients (see Fig. 13). Apart from C_{v1} , none of the other parameters seemed to have considerable effect on the flow properties in the flow field. Therefore, the C_{v1} coefficient is retained as the epistemic uncertain parameter in the CFD problem along with aleatory variables Mach number and the angle of attack. The input uncertainty information for RAE 2822 transonic airfoil case is given in Table 12.

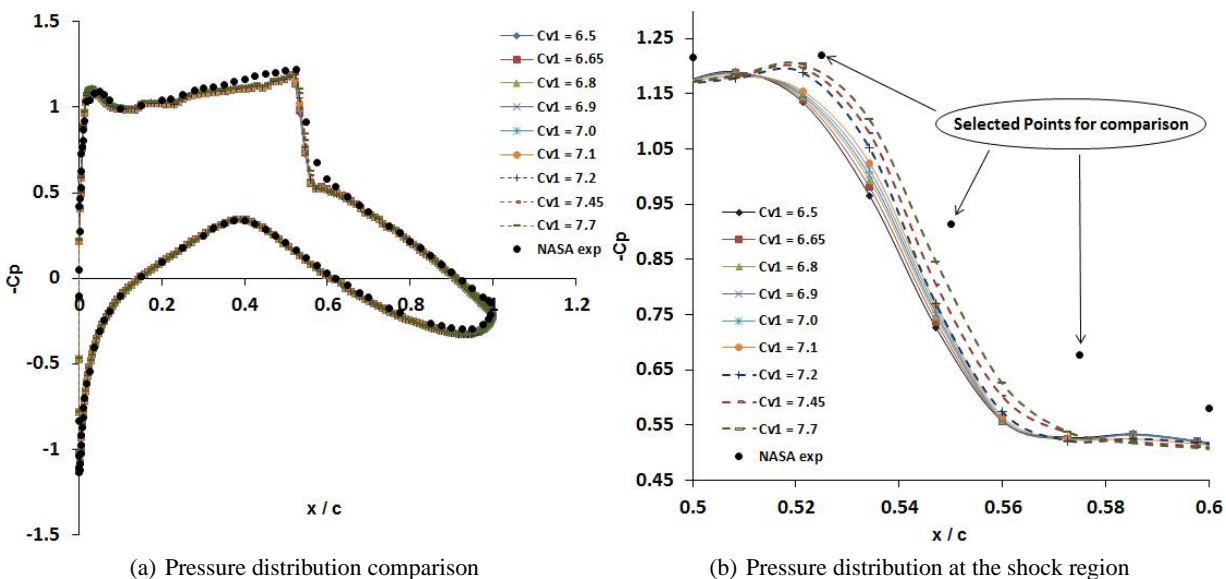


FIG. 13: Variation in C_p due to variation in C_{v1} in Spalart-Allmaras turbulence model.

TABLE 12: Uncertainty information for RAE 2822: transonic airfoil case

Variable	Uncertainty type	Uncertainty information
M	Aleatory	$N(0.725, 0.005)$
C_{v1}	Epistemic	$[6.5, 7.7]$
α	Aleatory	$N(2.92, 0.1)$

7.2.3 Determination of DSTE structure for the Epistemic Variable

The information for the epistemic variable can have different sources such as an expert opinion which states that the value of a particular variable will lie within a single interval or multiple intervals. Another source of information can be the data obtained from experiments. Evidence theory provides the tools required to incorporate the information from different sources. In the present analysis, evidence (uncertainty information) for C_{v1} is acquired from two different sources: (1) expert opinion from the literature, and (2) the comparison of numerical simulations to the selected experimental data.

Spalart and Allmaras [26] preferred the value of C_{v1} as 7.1 instead of Mellor and Herring's [33] 6.9, which they believe yields a low intercept for the log law. The proposed value of C_{v1} is validated by different researchers to be accurately calibrated using different methods, especially for boundary layer flows. Based on these analyses, for demonstration purposes the epistemic interval in Table 12 is segregated into three subintervals: [6.5, 6.85], [6.85, 7.15], and [7.15, 7.7]. Note that the sub-intervals do not need to be continuous but can also be overlapping or discontinuous in the application of the evidence theory. As the values of 6.9 and 7.1 both lie within the second interval, 100% BPA is assigned to that particular interval on the basis of expert opinion from literature review.

The second source of information regarding the uncertain parameter has been obtained from the comparison of the CFD simulations with different values of C_{v1} in the selected intervals to the available experimental data. The following procedure is adopted in order to derive an error-based BPA assignment for each subinterval k where $k = 1, 2, \dots, N_{int}$ ($N_{int} = 3$ in the present study):

1. Three different C_{v1} values have been chosen from each subinterval (two values close to the upper and lower bounds and the third value approximately at the mean of that particular interval). Let j denote the index of the CFD simulation for each subinterval where $j = 1, 2, \dots, N_{CFD}$ with $N_{CFD} = 3$ for each interval in the present analysis.
2. As the maximum deviation is observed in the shock region, we select three points ($x/c = 0.525, 0.55, 0.575$) for comparison with the experimental results as shown in Fig. 13(2). Let i denote the index for the number of points selected to be compared with the experimental results for each subinterval where $i = 1, 2, \dots, N_{exp}$ ($N_{exp} = 3$ in the present analysis).
3. Error ϵ_k as a function of coefficient of pressure C_p on the upper surface at the selected points for comparison can be given by:

$$\epsilon_k = \frac{1}{N_{CFD}} \left\{ \sum_{j=1}^{N_{CFD}} \sqrt{\frac{\sum_{i=1}^{N_{exp}} [((Cp_{exp})_{ij})_k - ((Cp_{CFD})_{ij})_k]^2}{N_{exp}}} \right\}. \quad (25)$$

4. Weights (ω_k) are assigned to each subinterval on the basis of error value evaluated, $\omega_k = 1/\epsilon_k$.
5. BPA's can now be assigned to each subinterval by normalizing the weights with the cumulative weight which can be mathematically expressed as:

$$BPA_k = \frac{\omega_k}{\sum_{k=1}^{N_{int}} \omega_k}. \quad (26)$$

The DSTE structure for the epistemic variable C_{v1} obtained through the stepwise procedure explained above is outlined in Table 13.

TABLE 13: Uncertainty information for the epistemic variable C_{v1}

Source	BPA		
	[6.5, 6.85]	[6.85, 7.15]	[7.15, 7.7]
1	29.40%	31.68%	38.91%
2	100%		

7.2.4 UQ Results

Following the observations made in Section 6, the aleatory variables were discretized into 50 subintervals in the mixed UQ analysis of this CFD problem. Three output quantities have been monitored in the airfoil case study, namely, coefficient of pressure (C_p) on the airfoil surface, coefficient of lift (c_l) and coefficient of drag (c_d). NIPC response surface is used as a surrogate for each output quantity and DSTE results in the form of belief and plausibility have been derived. The surrogate model was created with a first-, second-, and third-order NIPC expansion with an over-sampling ratio of 2, which required 8, 20, and 40 deterministic CFD evaluations respectively.

The convergences of NIPC expansion orders in terms of uncertainties in lift and drag coefficient are shown in Fig. 14. They can be interpreted as lower (plausibility) and upper (belief) bounds similar to the second-order probability analysis for each polynomial order. For example, the probability of $c_l \leq 0.82$ is between 0.25 (indicated by third-order CBF) and 0.4 (indicated by third-order CPF). These quantities are not affected much by the epistemic parameter C_{v1} which is evident from the width of the probability box (region between the belief and plausibility curves). This is in accordance with the turbulence model parameter studies which show that the closure coefficient, C_{v1} does not significantly affect the flow properties at lower angles of attack where there is minimal separation of flow. Evidently, the results may be different if we perform the analysis at higher angles of attack.

In the case of C_p , uncertainty is represented in terms of error bars which is similar to the documentation standards for experimental data, using a third-order NIPC expansion at each point. The third-order expansion is created at 296 different points on the airfoil surface using the same 40 deterministic function evaluations, i.e., CFD runs utilized in the analysis of c_l and c_d for each surface pressure coefficient. Belief and plausibility curves are generated at each point using the corresponding surrogate model. The 95% CI is obtained using the response value at 2.5% plausibility level and 97.5% belief level as shown in Fig. 15. It is clear that the maximum uncertainty is in the shock region and the changing shock wave location varies the pressure distribution denoted by the length of uncertainty bars. Note that

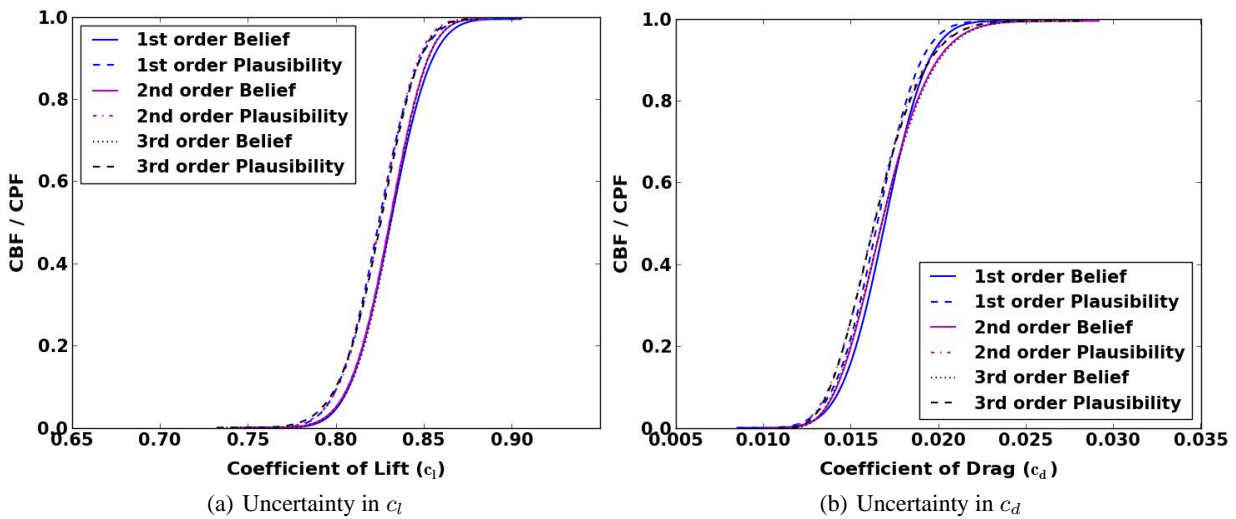


FIG. 14: UQ using mixed DSTE results for c_l and c_d .

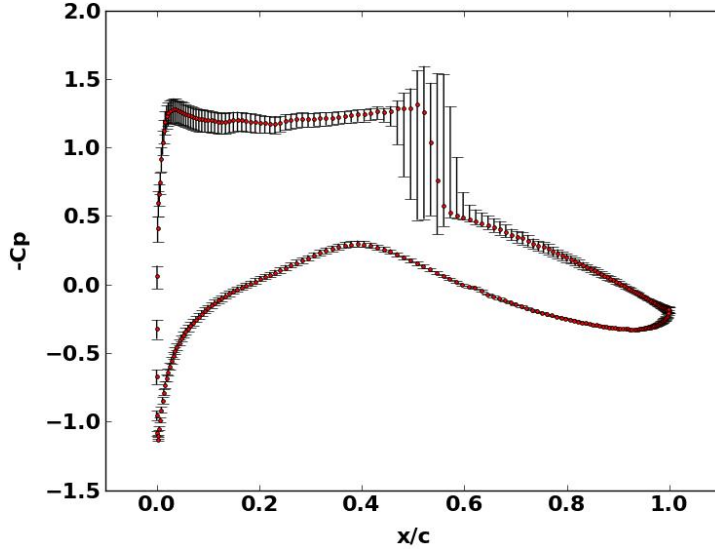


FIG. 15: UQ using mixed DSTE results for C_p .

the local oscillations in the shock region are likely due to the global polynomial approximation of the large gradients present in the flow field. Hence application of local approximation methods can also be considered for uncertainty quantification in regions of discontinuity.

Further, to quantify the individual contribution of each uncertain parameter to the uncertainty in c_l and c_d , Sobol indices [34] were evaluated. The basic procedure to calculate the Sobol index for a particular variable is explained in the Appendix. The sensitivity results for c_l and c_d for NIPC orders 1, 2, and 3 are provided in Table 14. As expected, the angle of attack ($\tilde{\alpha}$) is the highest contributor followed by Mach number (M) and C_{v1} in terms of coefficient of lift, whereas the Mach number contributes more towards the uncertainty in coefficient of drag as compared to $\tilde{\alpha}$. The variation in Sobol indices for the epistemic parameter C_{v1} for both output quantities are in accordance with the uncertainty plots in Fig. 15 with the uncertainty range being wider for c_l as compared to c_d .

8. CONCLUSIONS

In this paper, we have presented an approach for mixed UQ with evidence theory and stochastic expansions. The aleatory variables are discretized into sets of intervals with appropriate BPA's according to their probability distributions. They are treated as well characterized epistemic variables in the DSTE analysis. Also, the point-collocation NIPC has been implemented for construction of a stochastic surrogate model with the overall objective of reducing original function evaluations and achieving computational efficiency.

TABLE 14: Sobol indices for the uncertain input parameters for coefficient of lift and drag

Uncertain parameter	Coefficient of lift (c_l)			Coefficient of drag (c_d)		
	First-order NIPC	Second-order NIPC	Third-order NIPC	First-order NIPC	Second-order NIPC	Third-order NIPC
Mach number (M)	0.1149	0.1042	0.1002	0.7514	0.7505	0.7450
C_{v1}	0.0145	0.0107	0.0188	0.0011	0.00085	0.00047
Angle of attack ($\tilde{\alpha}$)	0.8706	0.8891	0.8951	0.2475	0.2650	0.2766

A detailed analysis is carried out in order to quantify the optimum number of subintervals required to accurately represent an aleatory domain. In this study, we focus on normal and uniform distributions for the aleatory variables. A minimum number of subintervals in case of 1, 2, 4, 6, and 8 aleatory variables in a specific problem have been recommended as 75, 50, 40, 18, and 12 intervals per aleatory variable, respectively. Also, the effect of distributions on the number of intervals required has been discussed.

The mixed UQ using, NIPC based DSTE approach and verification of the proposed minimum number of intervals for aleatory discretization is demonstrated using two examples: (1) three-variable Rosenbrock function and (2) transonic flow over RAE 2822 airfoil.

The first model problem (Rosenbrock function) was modeled with multiple sources of uncertainty for the epistemic variable. A fourth-order chaos expansion was chosen for propagation of input uncertainty using DSTE analysis. The normal variable was modeled with 20 intervals whereas the uniform variable was modeled with 30 intervals (a total of 50 intervals) representing the aleatory domain for the model problem. This was found to be in accordance with the numerical analysis carried out for optimum number of subintervals.

For our second model problem, the mixed UQ approach is demonstrated on the transonic CFD study of the airfoil (RAE 2822). Mach number and angle of attack are treated as aleatory and the closure coefficient C_{v1} in the Spalart-Allmaras turbulence model is treated as the epistemic uncertainty. A method to derive BPA's for the epistemic variable based on expert opinion and comparison between experimental data and CFD simulations is demonstrated. Since both aleatory variables are normally distributed, 50 intervals are used to discretize the aleatory domain. The epistemic parameter did not have a major contribution in the output uncertainty which was clear from the Sobol indices and is also in accordance with the previous findings that variation in C_{v1} has minimal effect at lower angles of attack.

Overall, the examples demonstrated that the NIPC based evidence theory is capable of capturing mixed uncertainty in the case of multiple sources of uncertainty for epistemic variables. It was also shown that global bound approximation for the epistemic variable by neglecting the sources of uncertainty with beliefs can lead to overestimation of the output uncertainty. Future research will include application of the proposed approach for large scale problems by implementing the sensitivity analysis based dimension reduction techniques.

ACKNOWLEDGMENTS

This research was supported by NASA Jet Propulsion Laboratory under a Small Business Technology Transfer Phase II project grant no. NNX11CC60C (Lee D. Peterson, program manager).

REFERENCES

1. Oberkampf, W. L., Diegert, K., V., Alvin, K., F., and Rutherford, B., M., Variability, uncertainty and error in computational simulation, *In ASME Proceedings of the 7th AIAA/ASME Joint Thermophysics and Heat Transfer Conference*, 357(2):259–272, 1998.
2. Shafer, G., *A Mathematical Theory of Evidence*, Princeton University Press, Princeton, NJ, 1976.
3. Zadeh, L. A., review of books: A mathematical theory of evidence, *AI Magazine*, 5(3):81–83, 1984.
4. Zadeh, L. A., A simple view of the Dempster Shafer theory of evidence and its implication for the rule of combination, *AI Magazine*, 7:85–90, 1986.
5. Yager, R., Arithmetic and other operations on Dempster Shafer structures, *Int. J. Man-Mach. Stud.*, 25:357–366, 1986.
6. Helton, J. C., Johnson, J. D., and Oberkampf, W. L., An exploration of alternative approaches to the representation of uncertainty in model predictions, *Reliab. Eng. Syst. Saf.*, 85:39–71, 2004.
7. Oberkampf, W. L., Helton, J. C., Joslyn, C. A., Wojtkiewicz, S. F., and Ferson, S., Challenge problems: Uncertainty in system response given uncertain parameters, *Reliab. Eng. Syst. Saf.*, 85(1-3):11–19, 2004.
8. Bae, H., Grandhi, R. V., and Canfield, R. A., An approximation approach for uncertainty quantification using evidence theory, *Reliab. Eng. Syst. Saf.*, 86:215–225, 2004.
9. Bae, H., Grandhi, R. V., and Canfield, R. A., Epistemic uncertainty quantification techniques including evidence theory for large-scale structures, *Reliab. Eng. Syst. Saf.*, 82:1101–1112, 2004.

10. Agarwal, H., Renaud, J. E., and Padmanabhan, D., Uncertainty quantification using evidence theory in multidisciplinary design optimization, *Reliab. Eng. Syst. Saf.*, 85:281–294, 2004.
11. Eldred, M. S. and Swiler, L. P., *Efficient Algorithms for Mixed Aleatory-Epistemic Uncertainty Quantification with Application to Radiation-Hardened Electronics*, Sandia National Laboratories SAND2009-5805, Albuquerque, NM, September 2009.
12. Eldred, M. S., Swiler, L. P., and Tang, G., Mixed aleatory-epistemic uncertainty quantification with stochastic expansions and optimization-based interval estimation, *Reliab. Eng. Syst. Saf.*, 96:1092–1113, 2011.
13. Hosder, S., Walters, R. W., and Balch, M., Efficient sampling for nonintrusive polynomial chaos applications with multiple input uncertain variables, *In Proc. of 9th AIAA Non-Deterministic Approaches Conference*, AIAA Paper 2007-1939, Honolulu, HI, April 2007.
14. Hosder, S., Walters, R. W., and Balch, M., Point-collocation nonintrusive polynomial chaos method for stochastic computational fluid dynamics, *AIAA J.*, 48(12):2721–2730, 2010.
15. Bettis, B. R., Hosder, S., and Winter T., Efficient uncertainty quantification in multidisciplinary analysis of a reusable launch vehicle, *In Proc. of 17th AIAA International Space Planes and Hypersonic Systems and Technologies Conference*, AIAA Paper 2011-2393, San Francisco, CA, April 2011.
16. Hosder, S., Stochastic response surfaces based on nonintrusive polynomial chaos for uncertainty quantification, *Int. J. Math. Model. Numer. Opt.*, 3(1–2):117–139, 2012.
17. Hosder, S. and Bettis, B. R., Uncertainty and sensitivity analysis for reentry flows with inherent and model-form uncertainties, *J. Spacecr. Rockets*, 49(2):193–206, 2012.
18. Oberkampf, W. L., Helton, J. C., and Sentz, K., Mathematical representation of uncertainty, *In Proc. of 3rd Non-Deterministic Approaches Forum*, AIAA Paper 2001-1645, Seattle, WA, April 2001.
19. Nikolaidis, E., Ghiocel, D. M., and Singhal, S., *Engineering Design Reliability Handbook*, 1st ed., Boca Raton, FL, CRC Press, 2004.
20. Sentz, K. and Ferson, S., *Combination of Evidence in Dempster Shafer Theory*, Sandia National Laboratories SAND2002-0835, Albuquerque, NM, 2002.
21. Akram, F., Prior, M. A., and Mavris, D. N., A comparison between monte carlo and evidence theory approaches for technology portfolio planning, *Infotech@Aerospace 2011*, AIAA Paper 2011-1412, St. Louis, MO, March 2011.
22. Helton, J. C., Johnson, J. D., Oberkampf, W. L., and Storlie, C., B., A sampling-based computational strategy for the representation of epistemic uncertainty in model predictions with evidence theory, Sandia National Laboratories SAND2006-5557, Albuquerque, NM, October 2006.
23. Byrd, R. H., Lu, P., and Nocedal, J., A limited memory algorithm for bound constrained optimization, *SIAM J. Sci. Stat. Comput.*, 16(5):1190–1208, 1995.
24. Witteveen, J. A. S., Doostan, A., Chantrasmi, T., Pecnik, R., and Iaccarino, G., Comparison of stochastic collocation methods for uncertainty quantification of the transonic RAE 2822 airfoil, Workshop on Quantification of CFD Uncertainties, Vrije Universiteit Brussel, Brussels, Belgium.
25. ANSYS FLUENT, Tutorial Guide, version 14.5, ANSYS Inc., Southpointe, 275 Technology Drive, Canonsburg, PA 15317, 2011.
26. Spalart, P. R. and Allmaras, S. R., A one-equation turbulence model for aerodynamic flows, *In Proc. of 30th Aerospace Sciences Meeting and Exhibit*, AIAA Paper 92-0439, Reno, NV, January 1992.
27. Cook, P. H., McDonald, M. A., and Firmin, M. C. P., Aerofoil RAE 2822—Pressure distributions, boundary layer and wake measurements, *Experimental Database for Computer Program Assessment*, AGARD Report AR 138, 1979.
28. Hosder, S., Grossman, B., Haftka, R. T., Mason, W. H., and Watson, L. T., Quantitative relative comparison of CFD simulation uncertainties for a transonic diffuser problem, *Comput. Fluids*, 35:1444–1458, 2006.
29. Kato, H. and Obayashi, S., Approach for uncertainty of turbulence modeling based on data assimilation technique, *Comput. Fluids*, 85:2–7, 2013.
30. Godfrey, A. G. and Cliff, E. M., Sensitivity equations for turbulent flows, *In Proc. of 39th Aerospace Sciences Meeting and Exhibit*, AIAA Paper 2001-1060, Reno, NV, January 2001.
31. Rhee, M., Evaluation of grid convergence and turbulence model constant changes for the airfoil flow simulation, *In Proc. of 45th AIAA Aerospace Sciences Meeting and Exhibit*, AIAA Paper 2007-1082, Reno, NV, January 2007.

32. Cheung, S. H., Oliver, T. A., Prudencio, E. E., Prudhomme, S., and Moser, R. D., Bayesian uncertainty analysis with applications to turbulence modeling, *Reliab. Eng. Syst. Saf.*, 96:1137–1149, 2011.
33. Mellor, G. L. and Herring, H. J., Two methods of calculating turbulent boundary layer behavior based on numerical solution of the equations of motion, *Proc. AFOSR-IFP Standard Conf.*, 1:275–299, 1968.
34. Sobol, I., Global sensitivity indices for nonlinear mathematical models and their Monte Carlo estimates, *Math. Comput. Simulation*, 55:271–280, 2001.
35. Sudret, B., Global Sensitivity analysis using polynomial chaos expansion, *Reliab. Eng. Syst. Saf.*, 93(7):964–979, 2008.
36. Crestaux, T., Maitre, O. L., and Martinez, J. M., Polynomial chaos expansion for sensitivity analysis, *Reliab. Eng. Syst. Saf.*, 94(7):1161–1172, 2009.
37. Ghaffari, S., Magin, T., and Iaccarino, G., Uncertainty quantification of radiative heat flux modeling for titan atmospheric entry, *In Proc. of 48th AIAA Aerospace Sciences Meeting*, AIAA Paper 2010-239, Orlando, FL, January 2010.

APPENDIX A. GLOBAL SENSITIVITY ANALYSIS WITH SOBOL INDICES

In a system where multiple uncertain variables are present, it is often useful to demonstrate and rank the relative importance of each input uncertain variable to the overall output quantity of interest using a global sensitivity analysis approach. In the current study, Sobol [34] indices are used to perform this analysis. Sobol indices can be derived via *Sobol decomposition* which is a variance-based global sensitivity analysis method. First, the total variance (D) can be written in terms of the PCE as follows:

$$D = \sum_{j=1}^P \alpha_j^2(t, \vec{x}) \left\langle \Psi_j^2(\vec{\xi}) \right\rangle. \quad (\text{A.1})$$

Next, as shown by Sudret [35] and Crestaux et al. [36], the total variance can be decomposed as:

$$D = \sum_{i=1}^{i=n} D_i + \sum_{1 \leq i < j \leq n}^{i=n-1} D_{i,j} + \sum_{1 \leq i < j < k \leq n}^{i=n-2} D_{i,j,k} + \cdots + D_{1,2,\dots,n}, \quad (\text{A.2})$$

where the partial variances (D_{i_1, \dots, i_s}) are given by:

$$D_{i_1, \dots, i_s} = \sum_{\beta \in \{i_1, \dots, i_s\}} \alpha_{\beta}^2 \left\langle \Psi_{\beta}^2(\vec{\xi}) \right\rangle, \quad 1 \leq i_1 < \dots < i_s \leq n. \quad (\text{A.3})$$

Further, the Sobol indices ($S_{i_1 \dots i_s}$) are defined as:

$$S_{i_1 \dots i_s} = \frac{D_{i_1, \dots, i_s}}{D}, \quad (\text{A.4})$$

which satisfy the following equation:

$$\sum_{i=1}^{i=n} S_i + \sum_{1 \leq i < j \leq n}^{i=n-1} S_{i,j} + \sum_{1 \leq i < j < k \leq n}^{i=n-2} S_{i,j,k} + \cdots + S_{1,2,\dots,n} = 1.0. \quad (\text{A.5})$$

The Sobol indices provide a sensitivity measure due to individual contribution from each input uncertain variable (S_i), as well as the mixed contributions ($\{S_{i,j}\}$, $\{S_{i,j,k}\}$, \dots). As shown by Sudret [35] and Ghaffari et al. [37], the total (combined) effect (S_{T_i}) of an input parameter i is defined as the summation of the partial Sobol indices that include the particular parameter:

$$S_{T_i} = \sum_{L_i} \frac{D_{i_1, \dots, i_s}}{D}; \quad L_i = \{(i_1, \dots, i_s) : \exists k, 1 \leq k \leq s, i_k = i\}. \quad (\text{A.6})$$

For example, with $n = 3$, the total contribution to the overall variance from the first uncertain variable ($i = 1$) can be written as:

$$S_{T_1} = S_1 + S_{1,2} + S_{1,3} + S_{1,2,3}. \quad (\text{A.7})$$

From these formulations, it can be seen that the Sobol indices can be used to provide a relative ranking of each input uncertainty to the overall variation in the output with the consideration of nonlinear correlation between input variables and output quantities of interest.